

University of Windsor

Scholarship at UWindor

Electronic Theses and Dissertations

Theses, Dissertations, and Major Papers

4-13-2017

Generic Thermodynamic Template for Expander Performance

Luka Celic

University of Windsor

Follow this and additional works at: <https://scholar.uwindsor.ca/etd>

Recommended Citation

Celic, Luka, "Generic Thermodynamic Template for Expander Performance" (2017). *Electronic Theses and Dissertations*. 5931.

<https://scholar.uwindsor.ca/etd/5931>

This online database contains the full-text of PhD dissertations and Masters' theses of University of Windsor students from 1954 forward. These documents are made available for personal study and research purposes only, in accordance with the Canadian Copyright Act and the Creative Commons license—CC BY-NC-ND (Attribution, Non-Commercial, No Derivative Works). Under this license, works must always be attributed to the copyright holder (original author), cannot be used for any commercial purposes, and may not be altered. Any other use would require the permission of the copyright holder. Students may inquire about withdrawing their dissertation and/or thesis from this database. For additional inquiries, please contact the repository administrator via email (scholarship@uwindsor.ca) or by telephone at 519-253-3000ext. 3208.

Generic Thermodynamic Template for Expander Performance

by

Luka Celic

A Thesis

Submitted to the Faculty of Graduate Studies
through the Department of Mechanical, Automotive & Materials Engineering
in Partial Fulfillment of the Requirements for
the Degree of Master of Applied Science at the
University of Windsor

Windsor, Ontario, Canada

2017

© 2017 Luka Celic

Generic Thermodynamic Template for Expander Performance

by

Luka Celic

APPROVED BY:

Dr. R. Carriveau
Civil and Environmental Engineering

Dr. V. Stoilov
Mechanical, Automotive & Materials Engineering

Dr. A. Sobiesiak, Advisor
Mechanical, Automotive & Materials Engineering

January 23, 2016

Declaration of Originality

I hereby certify that I am the sole author of this thesis and that no part of this thesis has been published or submitted for publication.

I certify that, to the best of my knowledge, my thesis does not infringe upon anyone's copyright nor violate any proprietary rights and that any ideas, techniques, quotations, or any other material from the work of other people included in my thesis, published or otherwise, are fully acknowledged in accordance with the standard referencing practices. Furthermore, to the extent that I have included copyrighted material that surpasses the bounds of fair dealing within the meaning of the Canada Copyright Act, I certify that I have obtained a written permission from the copyright owner(s) to include such material(s) in my thesis and have included copies of such copyright clearances to my appendix.

I declare that this is a true copy of my thesis, including any final revisions, as approved by my thesis committee and the Graduate Studies office, and that this thesis has not been submitted for a higher degree to any other University or Institution.

Abstract

As emissions regulations become more stringent, automakers must improve fuel consumption in their vehicles to meet performance targets. An Organic Rankine Cycle is a technology with substantial fuel savings potential. As the power producing device in the system, the expander is a critical component with a large impact on overall cycle efficiency. The choice of expander type can significantly affect system design choices. In order to decrease development time, a modeling tool which can evaluate the performance of various expander types is necessary to simulate expander performance without the need for costly prototyping and testing. This thesis will examine the development of a generic Matlab expander model which can replicate expander performance through a thermodynamic analysis. A modular approach to modeling allows for differentiation between expander types and sizes through modification of user defined modules. Thermal behaviour of the device is examined with an emphasis on heat transfer and its effect on expander performance. Results of the model and applications including the system response to thermal conditions are examined in detail.

Acknowledgements

This thesis is the result of a two year collaborative double degree program through the University of Windsor and Politecnico di Torino in conjunction with industry partner Fiat Chrysler Automobiles. There are many people who represent these institutions who have made this work possible. I would like to express my appreciation to all of the people involved in the program from both a technical and administrative role. I would like to thank Dr. Andrzej Sobiesiak, Dr. Jennifer Johrendt, Prof. Giovanni Belingardi, Mohammed Malik, Angela Haskell, and Raffaella Fiora for their coordination and assistance throughout the program.

I would like to thank my advisors from FCA who provided valuable assistance and helped guide me through the difficult technical challenges I faced. I am grateful for the help of Vetrivel Chandrasekaran, Kevin Laboe, Federica Bettoja, and Mauro Casella for their patience and assistance. A special thank you goes to Dr. Tim Scott, who spent countless hours assisting me with my thesis and made this possible. Your kindness and experience helped guide me through the completion of this project.

I would like to express my gratitude to my thesis supervisor Dr. Andrzej Sobiesiak for his help and guidance. I would also like to thank Prof. Ezio Spessa and my committee members, Dr. Vesselin Stoilov and Dr. Rupp Carriveau for their suggestions and help in refining and improving my work.

Finally, I would like to express my gratitude to my family - my mother, father and sister who have always been by my side. They have never doubted me and always believed in me. Thank you for your encouragement and dedication.

Contents

| | |
|-------------------------------------------|------------|
| Declaration of Originality | iii |
| Abstract | iv |
| Acknowledgements | v |
| List of Figures | ix |
| List of Tables | xi |
| Nomenclature | xii |
| 1 Introduction | 1 |
| 1.1 Problem Statement | 2 |
| 1.2 Objectives | 3 |
| 1.3 Methodology | 4 |
| 2 Literature Review | 6 |
| 2.1 Waste Heat Recovery (WHR) | 6 |
| 2.2 Organic Rankine Cycle (ORC) | 7 |
| 2.3 Advantages of ORC | 9 |
| 2.4 Expander Technology | 9 |
| 2.4.1 Piston Expander | 11 |
| 2.4.2 Rotary Vane Expander | 11 |
| 2.4.3 Screw Expander | 12 |
| 2.4.4 Scroll Expander | 13 |
| 2.5 Expander Thermodynamics | 14 |
| 2.5.1 Expansion Process | 14 |
| 2.5.2 Over and Under Expansion | 15 |

| | | |
|----------|--------------------------------------------------------------|-----------|
| 2.5.3 | Working Fluid Selection | 17 |
| 2.6 | Expander Modeling | 18 |
| 2.6.1 | Current Modeling | 19 |
| 3 | Model Development | 22 |
| 3.1 | Simulation Goals | 22 |
| 3.2 | Simulation Approach | 23 |
| 3.2.1 | Model Assumptions | 27 |
| 3.3 | Derivation of Governing Equations | 28 |
| 3.3.1 | Temperature and Pressure | 28 |
| 3.3.2 | Mass Flow Rate | 31 |
| 3.3.3 | Efficiencies | 31 |
| 3.3.4 | Heat Transfer | 33 |
| 3.4 | Modeling Process | 36 |
| 3.4.1 | Initial Operating Conditions | 36 |
| 3.4.2 | Initial Guesses | 37 |
| 3.4.3 | User Defined Functions (Volume, Port Surface Area) | 37 |
| 3.4.4 | Flow Rates | 42 |
| 3.4.5 | Heat Transfer Parameters | 43 |
| 3.4.6 | Numerical Integration | 43 |
| 3.4.7 | Convergence Check | 44 |
| 3.4.8 | Performance | 45 |
| 3.4.9 | Results Summary | 46 |
| 4 | Results | 47 |
| 4.1 | Modeling Objectives | 47 |
| 4.2 | Experimental Testing Setup | 49 |
| 4.3 | Experimental Testing Procedure | 51 |

| | | |
|----------|-----------------------------------------------------------------|------------|
| 4.4 | Part A - Analysis of Experimental Error | 52 |
| 4.4.1 | Note about Testing Results and Approach | 52 |
| 4.4.2 | Error Calculation Procedure | 53 |
| 4.4.3 | Calculated Results | 54 |
| 4.4.4 | Plots | 55 |
| 4.4.5 | Discussion | 58 |
| 4.5 | Part B - Adiabatic Assumption Investigation | 60 |
| 4.5.1 | Case 1 - Adiabatic | 62 |
| 4.5.2 | Case 2 - With Heat Transfer | 67 |
| 4.6 | Part C - Rotor and Casing Temperature vs. Performance | 71 |
| 4.6.1 | Case 1 - 300 K Ambient Temperature | 72 |
| 4.6.2 | Case 2 - 275 Ambient Temperature | 75 |
| 4.6.3 | Case 3 - 250K Ambient Temperature | 77 |
| 4.6.4 | Comparison of Performance | 80 |
| 4.6.5 | Summary | 82 |
| 4.6.6 | Time to Full Performance | 83 |
| 5 | Conclusion and Recommendations | 89 |
| 5.1 | Summary | 89 |
| 5.2 | Results and Recommendations | 91 |
| | Appendices | 93 |
| | References | 95 |
| | Vita Auctoris | 101 |

List of Figures

| | | |
|------|---------------------------------------------------|----|
| 2.1 | Organic Rankine Cycle Diagram | 8 |
| 2.2 | Rotary Vane Expander | 12 |
| 2.3 | Screw Expander | 13 |
| 2.4 | Scroll Expander Operation | 14 |
| 2.5 | Expansion Process | 15 |
| 2.6 | Under (Left) and Over (Right) Expansion | 16 |
| 2.7 | Test Result Template 2 | 17 |
| 2.8 | Lemort Model Architecture | 20 |
| 3.1 | Model Setup | 23 |
| 3.2 | Generic Template | 25 |
| 3.3 | Heat Transfer Components Diagram | 27 |
| 3.4 | Process Flow Chart | 36 |
| 3.5 | Gas Space Volume Relationship | 38 |
| 3.6 | Port Surface Areas | 40 |
| 3.7 | Modifiable Function | 41 |
| 4.1 | ORC Test Setup Diagram | 50 |
| 4.2 | Error Analysis 1000 RPM | 56 |
| 4.3 | Error Analysis 1500 RPM | 56 |
| 4.4 | Error Analysis 2000 RPM | 57 |
| 4.5 | Error Analysis 3000 RPM | 58 |
| 4.6 | Error Analysis 3500 RPM | 58 |
| 4.7 | Port Surface Areas | 62 |
| 4.8 | Cylinder Temperature and Pressure | 63 |
| 4.9 | Mass Flow Rates | 63 |
| 4.10 | P-V Diagram | 65 |
| 4.11 | P-V Diagram Losses Comparison | 66 |

| | |
|------------------------------------------------------------|----|
| 4.12 In Cylinder Temperature and Pressure 300K | 67 |
| 4.13 Convection Coefficient | 68 |
| 4.14 Rotor Temperature 300K Case | 69 |
| 4.15 Casing Temperature 300K Case | 69 |
| 4.16 Components Temperatures 300K | 70 |
| 4.17 Isentropic Efficiency 300K | 72 |
| 4.18 Power 300K | 73 |
| 4.19 Rotor and Casing Temperatures 300K | 74 |
| 4.20 Isentropic Efficiency 275K | 75 |
| 4.21 Power 275K | 76 |
| 4.22 Rotor and Casing Temperatures 275K | 77 |
| 4.23 Isentropic Efficiency 250K | 78 |
| 4.24 Power 250K | 78 |
| 4.25 Rotor and Casing Temperatures 250K | 79 |
| 4.26 Isentropic Efficiency Comparison | 80 |
| 4.27 Power Comparison | 81 |
| 4.28 Temperature Drop Across Expander Comparison | 82 |
| 4.29 Rotor Temperature Comparison | 85 |
| 4.30 250K Rotor Temperature | 86 |
| 4.31 275K Rotor Temperature | 86 |
| 4.32 300K Rotor Temperature | 87 |

List of Tables

| | | |
|-----|------------------------------------------------|----|
| 4.1 | Summary of Testing and Calculations | 55 |
| 4.2 | Testing Conditions | 61 |
| 4.3 | Test Cases | 61 |
| 4.4 | Adiabatic Results | 64 |
| 4.5 | Losses Comparison | 67 |
| 4.6 | Heat Transfer Performance Comparison | 71 |
| 4.7 | Comparison Summary | 83 |
| 4.8 | Summary of Warm-up Times | 87 |

Nomenclature

- a first enthalpy coefficient
- A_{casing} casing area
- A_d discharge area
- A_{InPort} inlet port enclosure area
- A_{M2} secondary mass area
- $A_{OutPort}$ outlet port enclosure area
- A_{rotor} rotor area
- A_s surface area
- b second enthalpy coefficient
- B port area amplitude factor
- c third enthalpy coefficient
- C port area period factor
- C_c casing friction coefficient
- C_d discharge coefficient
- C_p specific heat at constant pressure
- C_R rotor friction coefficient
- C_v specific heat at constant volume
- d fourth enthalpy coefficient
- d_f frictional distance
- e fifth enthalpy coefficient
- E energy
- f sixth enthalpy coefficient
- f_f friction force
- h_1 enthalpy at state 1
- h_{2a} actual enthalpy at state 2
- h_{2s} isentropic enthalpy at stage 2

h_s suction enthalpy
 h_d discharge enthalpy
 h_{conv} heat transfer coefficient between fluid and metal
 h_o heat transfer coefficient between metal and ambient
 h_{vap} vapour enthalpy
 h_{sat} saturation enthalpy
 h_{liq} liquid enthalpy
 h_{fg} enthalpy change of evaporation
 h_{is} isentropic enthalpy
 k adiabatic index
 k_{cond} thermal conductivity
 L characteristic length
 m_s suction flow rate
 m_d discharge flow rate
 m_L leakage flow rate
 m_{actual} actual mass of refrigerant
 m_{ideal} ideal mass of refrigerant
 m_R mass of rotor
 m_C mass of casing
 m_{M2} mass of secondary mass
 m_{E2} mass of secondary mass envelop
 m_{in} mass of inlet port enclosure
 m_{out} mass of outlet port enclosure
 m_{new} new cycle mass
 m_{old} last cycle mass
 Nu Nusselt number
 P cylinder pressure

P_s suction pressure
 P_d discharge pressure
 P_{crit} critical pressure for choked flow
 P_{out} downstream pressure
 P_{in} upstream pressure
 P_{CR} fluid critical pressure
 P_{exp} expander power
 Pr Prandtl number
 Q heat energy
 Q_f friction heat energy
 R gas constant
 Re Reynolds number
 R_{rotor} rotor radius
 S_{vap} vapour entropy
 SH_{vap} vapour superheat
 T cylinder temperature
 T_{in} upstream temperature
 T_{out} downstream temperature
 t time
 t_{cycle} time of cycle
 t_{FP} time to full performance
 T_{sat} saturation temperature
 T_{new} new cycle temperature
 T_{old} last cycle temperature
 $T_{rotor,new}$ new cycle rotor temperature
 T_R rotor temperature
 T_{CR} critical temperature of fluid

T_C casing temperature
 T_{M2} secondary mass temperature
 T_{E2} envelope temperature
 T_{amb} ambient temperature
 T_{InPort} inlet port temperature
 $T_{OutPort}$ outlet port temperature
 u internal energy
 U fluid velocity
 V velocity
 V_c clearance volume
 V_d displacement volume
 W_a actual work
 W_{is} isentropic work
 x_{casing} casing thickness
 x_{gasket} gasket thickness
 x_n current x value
 x_{n+1} next x value
 x_{rotor} rotor thickness
 y_n current y value
 y_{n+1} next y value
 μ_d dynamic viscosity
 μ_s coefficient of friction
 η_{is} isentropic efficiency
 η_v volumetric efficiency
 η_m mechanical efficiency
 ρ cylinder density
 ρ_d discharge density

ρ_s suction density

τ time constant

ω angular velocity

θ crank angle

$\theta_{cutoff,in}$ inlet port cutoff angle

$\theta_{cutoff,out}$ outlet port cutoff angle

Abbreviations

ORC Organic Rankine Cycle

ICE Internal Combustion Engine

RPM Rotations Per Minute

WHRS Waste Heat Recovery System

OEM Original Equipment Manufacturer

1 Introduction

As stricter emissions regulations force original equipment manufacturers (OEM) to lower fuel consumption and emission levels, a particular emphasis is placed on the development of technologies which can enable reductions in these areas. One such technology is a Waste Heat Recovery System (WHRS) in the form of an Organic Rankine Cycle (ORC) sized for a vehicle application. As the costs of developing in-cylinder and after treatment solutions for emissions increase rapidly, OEM's have begun to look to WHR systems as a technology with large future potential for fuel savings. As much as 55-80%[1] of the energy produced by an internal combustion engine (ICE) is lost as heat through exhaust gases and coolant, and the recovery of a portion of this heat has the potential for substantial vehicle fuel economy improvement.

The most critical factor for optimizing overall cycle efficiency of such a system is the isentropic efficiency of the expander[2]. Maximizing the isentropic efficiency of the expansion device can result in significant increases in cycle efficiency and therefore the amount of power recovered from a low grade heat source. In order to be able to make design choices relating to the sizing and selection of expander type for a given ORC system, extensive testing and modeling of the system must take place. A virtual model which can predict the isentropic efficiency of a given expander geometry under a variety of operating conditions is a vital tool in exploring potential waste heat recovery solutions. Such a model can assist with design choices and give engineers an idea of the impact that expander type and geometry can have on the overall cycle efficiency of the system.

A modeling tool must take into account losses which cause inefficiencies within the device. Current models use an adiabatic assumption - that heat transfer losses in the expander are negligible in terms of performance. An investigation into heat transfer losses as a function of expander temperature can shed light on whether this assumption is valid and to what degree ambient temperature affects expander out-

put. In order to examine heat transfer losses, the thermal behaviour of each of the individual mechanical components of an expander must be examined.

1.1 Problem Statement

With strict new emissions regulations putting pressure on OEM's to reduce their exhaust emissions on a very tight time frames, there is a need to put innovative new technologies into production as quickly as possible. A necessary part of any research and development activity is virtual simulation, to both decrease the time spent in the design phase, and decrease the costs associated with developing expensive prototypes of the system. When making design choices for the next generation of ORC systems for on-board energy conversion, decisions on the expander type must be made. With many different kind of technologies flooding the market and all guaranteeing high performance, it is important to be able to compare different technologies to decide which will deliver the highest performance under the given operating conditions.

While empirical data and virtual models are widely available for evaluating mature technologies such as compressors, the relatively new field of waste heat recovery does not have widely available data or literature on expanders made specifically for this purpose. Quite often many systems employ compressors of various kinds acting as expanders by running in reverse [3]. While it is possible to run a compressor as an expander by removing various check valves and operating it backwards, often these types of expanders have detrimental performance [4] due to subtle but important differences in port design between compressors and expanders. A generalized, physics based tool for expander performance evaluation is a critical tool in the early design stages of the ORC system. A flexible model would allow for comparison between various technologies and provide insight into their operation under various operating conditions that may differ between systems. With the ability to analyze heat transfer losses within the expander, the model would allow for an investigation into the

performance of the expander with respect to its ambient temperature. The thermal behaviour of the mechanical components of the device is examined to observe their impacts on the working gas space temperature and thermal system response.

1.2 Objectives

The objective of this work is to create a generic expander simulation tool with 3 main goals:

1. Provide the ability to examine the performance of different expander types and geometries
2. Examine expander heat transfer through an analysis of the thermal behaviour of its mechanical components
3. Create a detailed physics-based model to be used as a benchmark for simpler models

This thesis describes in detail the development of a thermodynamic tool which provides these functionalities. Additionally, there are 3 main applications of the model which this document will examine. These applications demonstrate the usefulness of the model and its applicability to expander performance evaluation:

1. Assisting with error analysis in experimental testing
2. Verification of the adiabatic expander assumption
3. Investigation into the effects of ambient temperature on performance

The tool should be able to consider various expander types and geometries including piston, scroll, screw, and rotary vane type expanders. In fact, this requires that the model is generic – that it is modifiable according to which type of device is being

evaluated. Simulations are run at steady state conditions with constant inlet temperature and expander speed. No experimental testing was completed by the author. As will be discussed in the body of the thesis, the requirements for creating a very accurate model for a certain expander type requires two types of models [5]– the first is a geometric model which simulates the workings of the device in terms of its geometry – how the gas will flow through the device due to its specific physical characteristics. The second part is a thermodynamic model which predicts the performance characteristics of a given fluid as it travels through the expander as a function of its temperature, pressure, density, mass flow rate, and other thermodynamic variables. By having these two parts of an expander simulation in one model, the user can achieve a very high accuracy of simulation results as achieved by Lemort [6] with his scroll expander model. However, the development of such a model requires extensive research and development into geometric relationships of each kind of device – consider that a scroll expander can have 13 chambers which each need to be completely described geometrically for each revolution of the device.

This work will focus on the thermodynamic aspect of the expander model. This means that the model described in this thesis is considered a thermodynamic template for a generic expander model. Within the model, the user is given the ability to input geometric relationships for the working volume space in the expander (along with other physical parameters). Within this work the volume and port surface area relationships are assumed to be functions generally representative of generic expanders. A special focus on heat transfer losses in the expander will provide a basis for examining the degree to which heat transfer affects expander performance.

1.3 Methodology

The development of an expander model is based around the derivation of differential equations which describe the thermodynamic conditions inside the expansion

chamber. By starting with expressions for the conservation of mass and energy, the governing differential equations for the temperature and pressure can be developed. By solving these equations by integration through the crank angles of one revolution of the machine, expressions for the isentropic efficiency of the device can be solved. By also including heat transfer equations which describe the temperatures of all of the physically components found in modern expanders, the effects of the temperature of the lumped mass components on overall performance can be examined.

2 Literature Review

2.1 Waste Heat Recovery (WHR)

Increasing dependence on fossil fuels throughout the last 200 years has brought about consequences for the global environment. As a result of growing environmental problems, stricter emissions regulations are enforced on OEM's with the goal of reducing the harmful impact that vehicles have on the environment. Continuously stricter environmental regulations force OEM's to explore new technologies related to the improvement of fuel consumption and emissions.

Of particular importance are technologies which can convert already available energy to useful work without causing environmental pollution. One such area of research is Waste Heat Recovery Systems (WHRS) which are able to convert low grade heat sources to useful work [7]. Many such systems are available and typically consist of sources ranging between 80-350°C or up to 600°C [8], or where the size of the application is too small for a steam power plant . Examples of such applications are:

- Heat recovery from:
 - Low enthalpy geothermal sources exploitation (90-260 ° C)
 - Industrial processes (e.g. steel mills, glass mills, furnaces etc.)
 - Power generation (e.g. biogas, diesel, gas engines)
 - Gas compression stations
 - Biomass plants
 - Concentrated Solar Power (CSP)

2.2 Organic Rankine Cycle (ORC)

The most popular and widely used form of WHR is the Rankine Cycle [7]. An ideal Rankine cycle is a thermodynamic system which converts heat into mechanical work. The classic Rankine cycle employs water or steam as the working fluid and is typically found in large thermal power generation plants[9]. 90% of electricity capacity worldwide is generated through the Rankine cycle in various plants – nuclear, coal, oil, and biomass power plants employ Rankine cycle technology [5].

However, in order to employ the Rankine Cycle system on a smaller scale with lower grade heat sources, organic fluids are used in place of the traditional choice of water as working fluid. The choice of organic fluid greatly improves the performance and economic feasibility of the Rankine cycle system at low heat source temperatures. An Organic Rankine cycle replaces steam as the working fluid with an organic compound – a wide range of substances which contain at least one carbon atom. These organic fluids have a number of properties which greatly differ to those of water, making them advantageous for low temperature heat recovery. [10]The organic working fluid has a lower boiling point and a higher vapour pressure than water and is thus able to use low temperature heat sources to produce electricity. The fluid is chosen to best fit the heat source according to their differing thermodynamic properties, thus obtaining higher efficiencies[8]. A low boiling point temperature allows these fluids to be used at lower temperatures than steam, extending their range of applications far beyond those of a traditional steam Rankine cycle. These fluids can produce dry expansion – the fluid remains superheated throughout the expansion process and can result in less wear in the expander along with the ability to install additional components (recuperator) to increase overall cycle efficiency[11]. An ORC system is very flexible also in terms of power output – it can be applied to a number of power ranges anywhere from less than 1 kW (automotive applications) to the several MW range found in large industrial processes.

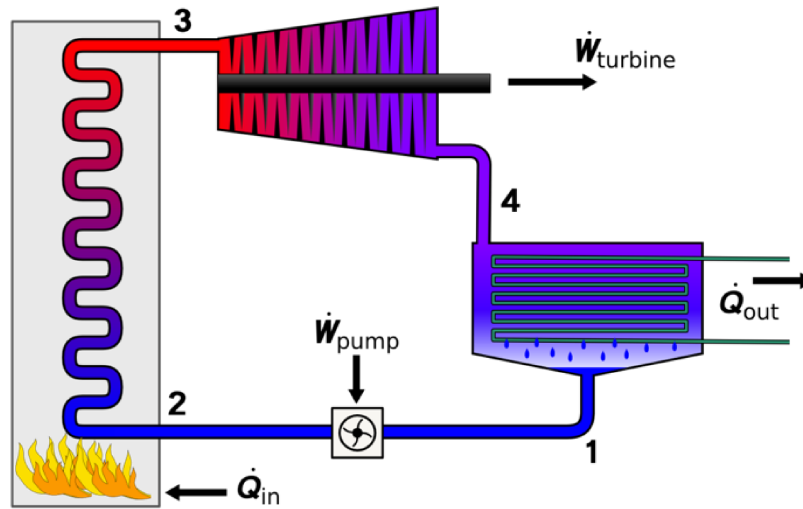


Figure 2.1: Organic Rankine Cycle Diagram

Figure 2.1 displays the setup of the ORC. The system consists of the 4 main components of the traditional steam Rankine cycle: the evaporator, expander, condenser and pump. Waste heat travels through the source and passes over a heat exchanger. The heat exchanger heats an intermediate fluid which cycles through the evaporator in a closed circuit. The organic fluid is vapourized by the heating from the intermediate fluid and enters the expander with a high temperature and pressure, where it is allowed to expand to create mechanical work. The vapour then exits the expander towards the condenser. Water from a cooling source condenses the vapour back into a fluid in a closed circuit. Once the system reaches the pump, it is pressurized to the required pressure and the system continues in a loop. A device called a recuperator is often used in the system to preheat (before entering the evaporator) and precool (before entering the condenser) the organic fluid, thus reducing the amount of heat needed to increase or decrease the temperature of the working fluid to its desired level, which increases overall system efficiency[12].

2.3 Advantages of ORC

The advantages of the ORC over the traditional Rankine cycle include[8]:

- Suitable for lower temperature applications
- Low rotation and tip speed, together with the absence of a liquid
- Single phase expansion leads to a reliable and long lasting expander
- Far simpler and lower cost maintenance than with a steam turbine
- Modular configuration for ease of transportation and installation
- Design flexibility with the option to utilize the most efficient working fluid available
- Operational flexibility for superior off-design performances
- High market availability of chemicals /fluids with refilling rarely required
- Low associated costs for foundation and assembly
- Simple and reliable system maintenance

2.4 Expander Technology

The power producing device in the ORC is the expander. The device operates by converting a pressure difference into mechanical work. Typically, the expander output shaft can be coupled to a generator to help power electrical components, or mechanically linked to the engine through a belt or pulley system. The efficiency of an ORC system is strongly dependent on the efficiency of the expander[13]. Expanders are divided into 2 main types: turbomachinery and positive displacement expanders.

Turbomachines use aerodynamic interactions with blades to create energy conversion. As summarized by Quoilin et al. [13], both axial and radial turbines are frequently used for large power applications (>100 MW). They can work at rotational speeds approaching 50,000 RPM and can have a wide range of efficiencies ranging between 60-90%. These high operational speeds require advanced manufacturing and design and their associated incurred costs. Additionally, there are a number of sensitivities which must be taken into account when considering turbomachines. Any liquid which has not been fully vapourized can cause permanent damage to the turbine blades, so special attention must be paid to make sure that the fluid is fully vapourized when entering and leaving the expander. This effect can be especially troublesome if any vapour partially condenses before completely leaving the turbine. Another hurdle to the proper implementation of turbines to small scale ORC's is the poor off design performance. A turbine can produce relatively high efficiencies at its design points, but when faced with constantly changing flow conditions such as the ones seen in automotive applications, efficiency can be very negatively affected with constantly changing mass flow rates and temperatures. Often, due to extremely high rotational speeds and the forces and vibrations that come with them, turbines require special lubrication along with more rugged seals and bearings, significantly contributing to their cost.

Positive displacement expanders instead use a closed, changing chamber volume to convert a pressure difference into mechanical work. These devices are typically used for small and medium grade power sources ranging from a few kW to 100 kW [5]. Compared to turbomachines, slower rotational speeds, higher expansion ratios, and lower costs can be expected with positive displacement expanders. While they display lower efficiencies in the peak operating range than turbines, they operate much better over a range of speeds and pressure ratios. Combined with lower costs associated with manufacturing, durability and reliability, expanders are more well suited to small scale

ORC applications than turbines[14]. There are many different kinds of expanders available for a variety of power ranges, each with a specific set of advantages and disadvantages. A few main types of positive displacement expanders include piston, rotary vane, scroll, and screw expanders. This thesis will examine the performance of positive displacement expanders which are more suitable for automotive applications.

2.4.1 Piston Expander

Piston expanders are in practice similar in operation to that of an IC engine without the combustion phase[11]. A piston expander has a unique characteristic which is the use of valves to control flow in and out of the device. Inlet and outlet (or suction and discharge) valves are used to control the processes in the form of sliding, poppet, or rotating valves to control the flow of fluid. This allows for precise timing and control of each of the processes, leading to flexibility in their control systems. However, precise timing and correct functionality of such a system adds to their complexity. Frictional losses in a piston expander can be significant due to the high level of friction between the piston rings and the cylinder[15].

Isentropic efficiencies for piston expander have been reported as high as 76%[37], but in most cases available in literature the experimentally determined efficiency is lower than 50%. [38, 39, 40, 16].

2.4.2 Rotary Vane Expander

A rotary vane expander is based on a number of vanes rotating along with a rotor to allow fluid to expand from the inlet port to the outlet port. A high temperature and pressure fluid enters the inlet port and its expansion forces rotational movement of the rotor and therefore an increase in the volume in the chamber, allowing expansion and the fluid to leave from the outlet port. As summarized by Imran[16], the rotary vane is a fairly simple device with a low number of parts, making it much less complicated

than many other expander types. This expander can operate with a very small mass flow rate, can operate with liquid formation in the flow, and has good NVH qualities. Similar to a piston machine, rotary vane expanders generally use valves to precisely control inlet and outlet refrigerant flows. Figure 2.2[17] displays the working principle of a rotary vane machine.

The highest isentropic efficiency reported for vane expander is 57%[41, 16], with isentropic efficiencies that can fall into the 40-50% range [42, 11].

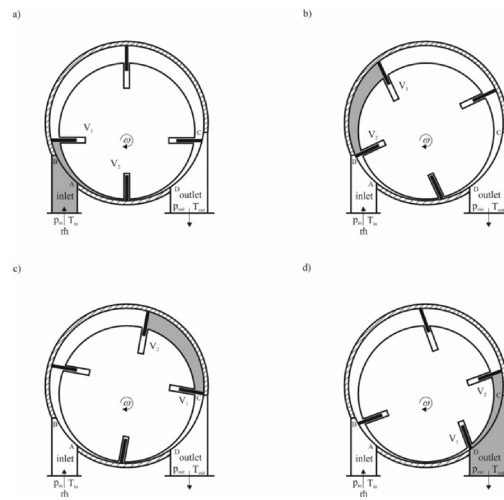


Figure 2.2: Rotary Vane Expander

2.4.3 Screw Expander

Screw expanders are devices based on interlocking helixes resembling a screw to allow a volume change within the device. A single screw system uses a single screw with two small gate rotors to allow expansion, while a twin screw system uses two screws which rotate inside overlapping cylinders[18]. The high pressure temperature gas entering the inlet port is allowed to expand in the region in between the elements and in turn forces them to rotate. A very important characteristic of screw expanders is the fact that the timing of the suction and discharge processes is imposed by the geometry of the machine. Contrary to a piston expander which provides the user with control of

the timing of inlet and outlet flows, the flow of refrigerant through the expander is determined by the conditions inside the expander itself. Figure 2.3[19] displays the operating principle behind a screw expander. Screw expander isentropic efficiencies can reach up to 70%[43, 44, 16].

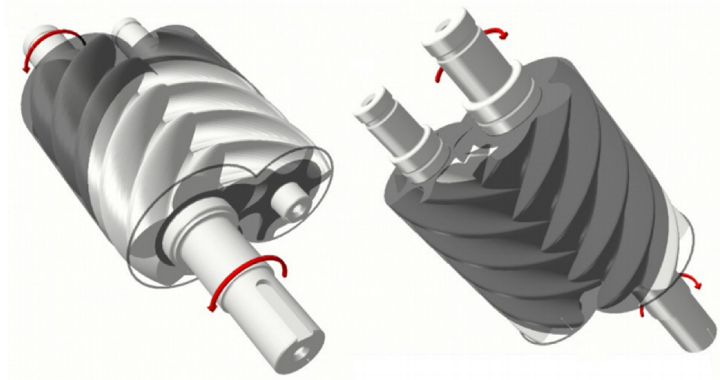


Figure 2.3: Screw Expander

2.4.4 Scroll Expander

A scroll expander uses two involute scrolls – one fixed and one rotating – which allow volume change within the chamber and therefore expansion of a gas. The two scrolls are offset in such a way that they create a number of pockets throughout the chamber. As the gas enters the inlet port at a high temperature and pressure, it moves outwards throughout the pockets of increasing volume and towards the outlet port, creating an orbital motion in the moving scroll.

The main advantages of this type of machine compared to conventional volumetric expanders are: a low number of components, few moving parts resulting in a high level of reliability, an ability to successfully work with a two-phase flow, low mechanical vibrations and pulsations implying a quasi-steady mechanical torque, and a quasi-continuous expansion process with an excellent volumetric efficiency[20]. Figure 2.4[11] displays the operating principle behind a scroll expander. Reported efficiencies have reached as high as 83%[45].

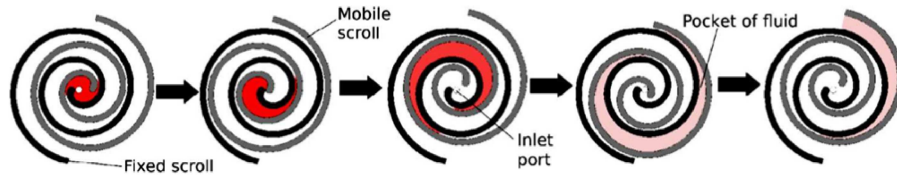


Figure 2.4: Scroll Expander Operation

2.5 Expander Thermodynamics

2.5.1 Expansion Process

For an expander operating at steady state conditions, the inlet state and outlet pressure are fixed. Therefore, the ideal process for an adiabatic expander is an isentropic process between the inlet state and the exhaust pressure [21]. The expansion process for a turbine is depicted in the h - S diagram in Figure 2.5[21] below. The high temperature, high pressure gas enters the expansion space where its pressure and temperature drop to the conditions at the expander exit. Losses which cause deviation from isentropic conditions include friction, leakage, and heat transfer, while changes in kinetic and potential energy are typically small and usually ignored.

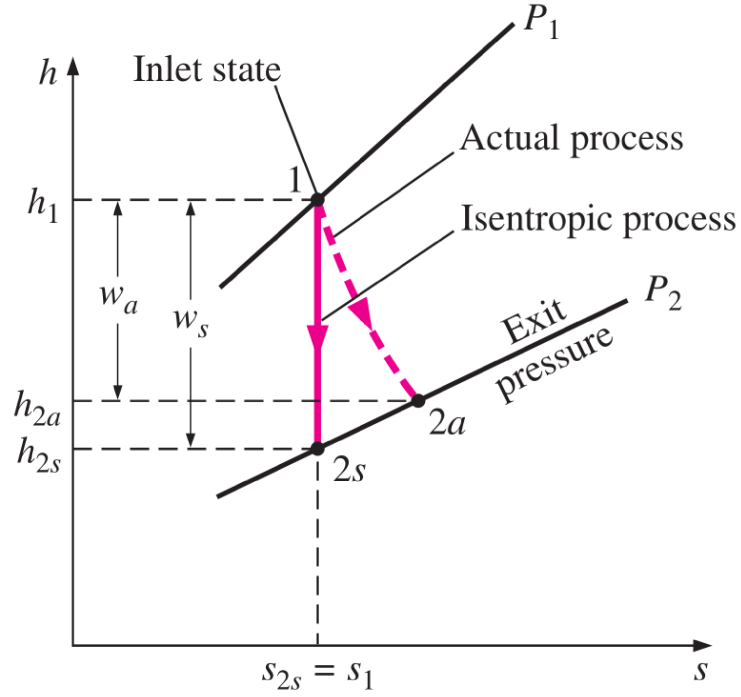


Figure 2.5: Expansion Process

The isentropic efficiency of a turbine is defined as the ratio of the actual work output of the turbine to the work output that would be achieved if the process between the inlet state and exit pressure were isentropic [21].

$$\eta_{is} = \frac{work_{actual}}{work_{isentropic}} = \frac{h_1 - h_{2a}}{h_1 - h_{2s}} \quad (2.1)$$

Where alternatively,

$$work_{actual} = \int PdV \quad (2.2)$$

2.5.2 Over and Under Expansion

If the volume ratio required by the system to match its desired operating conditions is not equal to the volume ratio of the expander, the result can be losses through over and under expansion as described by [13]. An expander volume ratio which is

lower than the system volume ratio will under-expand the gas, leading to a higher pressure at the end of the expansion process than that which is downstream of the expander. Similarly, an expander volume ratio greater than the system volume ratio will over-expand the gas, leading to a lower pressure in the expander than downstream conditions. The losses incurred as a result of both of these situations is depicted below in Figure 2.6[13].

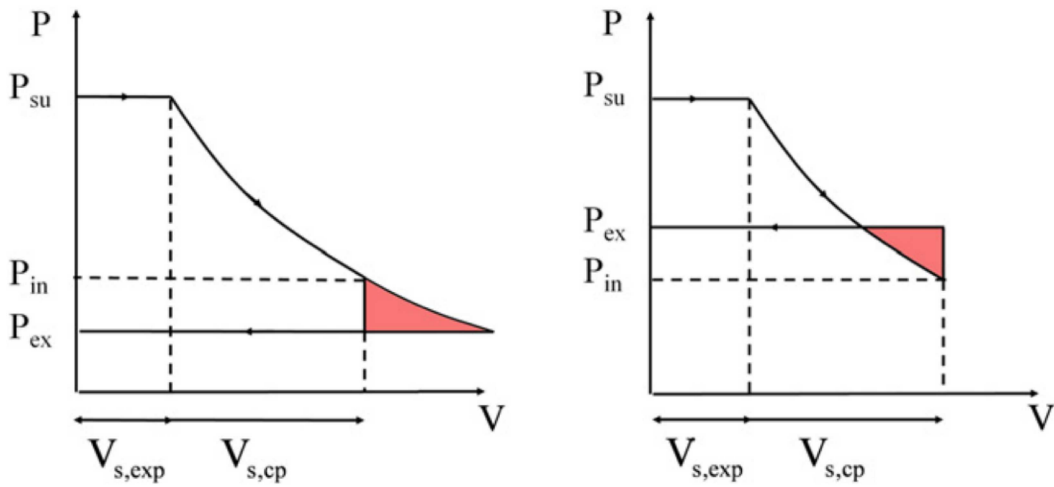


Figure 2.6: Under (Left) and Over (Right) Expansion

A goal of expander design is to avoid losses associated with over and under expansion by ensuring that the expander volume ratio is the same as the volume ratio required by the system to match its desired operating conditions. This is important when considering that many expanders tested today are actually compressors running in reverse as expanders. Since expansion ratios in Rankine cycle systems are typically larger than those in vapor compression systems, many of these systems incur substantial losses due to over/under expansion[22].

Most ORC designers will try to keep the pressure ratio near this maximum while also considering potential over and under expansion losses that can occur as a result of the pressure ratio selection. Figure 2.7 below depicts the optimum isentropic efficiency of the expander occurring at the expander design point. Losses at the design point

are due to leakage, friction, and heat transfer as opposed to over or under expansion of the working fluid. Hsu [49] shows that that this trend is found under varying operating conditions and can be applied to any expander type.

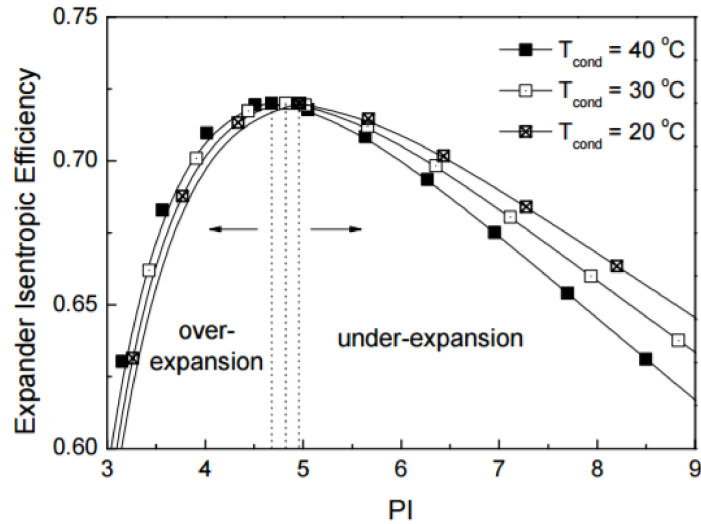


Figure 2.7: Test Result Template 2

2.5.3 Working Fluid Selection

Working fluid selection is one of the biggest factors affecting overall cycle efficiency and performance of an ORC system. The use of an organic working fluid as opposed to steam provides a number of advantages for low temperature waste heat recovery. There are a number of critical factors affecting the proper selection of a working fluid as described by Quoilin et al [13].

1. maximization of efficiency and output power for given temperatures through fluid characteristics such as: critical point, specific heat, density, etc.
2. positive or isentropic saturation vapor curve
3. High vapor density, low viscosity
4. Acceptable evaporating pressure – the higher the pressure, the higher the costs and complexity

5. High temperature stability
6. High safety level in terms of toxicity and flammability
7. Low ozone depleting potential (modern refrigerants very close to 0).
8. High availability and low cost

While literature covers a broad range of working fluids, there are only 6 few fluids currently commonly used[13]. These fluids are R-134, R245fa, n-pentane, Solkatherm, OMTS, and Toluene. For the purposes of this thesis, R245fa has been chosen as the working fluid.

2.6 Expander Modeling

When developing predictive expander models, there are two main criteria which must be fulfilled to get meaningful and accurate simulation results. The first criterion is a detailed analysis of the expander geometry. Of interest when modeling an expander is the change in chamber volume with time – how the expansion space evolves as the machine is in operation. In some cases, such an expression can be relatively simple to describe, such as with a piston expander as the working gas space has a simple and consistent shape. In other cases, like with a scroll or screw expander, the geometrical relationships can be very complex and difficult to describe mathematically. For example, a scroll expander can have 13 chambers [6] which each have a specific equation describing their respective volume evolution over a certain time interval – leading to considerably more complex equations to describe the overall path of gas through that expander type. Similarly, the overlapping of screws in a screw type expander can lead to many pockets of gas to be described independently and therefore a set of considerably complicated equations. It is clear that the geometric criteria for modeling is completely based on the expander type being investigated and will differ greatly from device to device.

The second criterion needed to create a modeling tool is the thermodynamic evolution of gases inside the working space. This involves describing the changes in temperature, pressure, enthalpy, volume, density and other thermodynamic variables throughout the expansion process in a given expander type. Equations describing these variables can be developed from the conservation of mass and energy equations, with geometrical data as a module used as an input into the thermodynamic equation module.

This means that the thermodynamic equations are solved on the basis of knowing the geometrical characteristics of the machine in question – the two parts of the larger model can be decoupled and solved separately. Equations describing temperature, pressure, etc. can be calculated the same way whether the input geometry of the machine is based on a scroll, screw, rotary vane, piston, or any other type of expander.

2.6.1 Current Modeling

Currently, expander technology is a relatively new field. Much of the literature that can be found on expander modeling actually applies to compressors or compressors running in reverse as expanders. However, many of those principles can be carried over to expander modeling.

A very comprehensive scroll expander model was developed by Lemort [6] with very high accuracy. The model is specific to a scroll expander and includes a detailed geometric model of 14 individual chambers in the scroll machine. Volume relationships are developed for each individual chamber as a function of time. Lemort built on the work of Halm[25] and Chen [27] who created a scroll compressor model. Lemort's work added expander operation and gave a detailed geometric relationship to a higher number of working chambers. Development of the governing physical equations was performed in terms of mass and internal energy, with enthalpies and efficiencies calculated on the basis of lookup tables once the equations were solved for

each revolution of the machine. The model architecture is displayed below in Figure 2.8[6]. It clearly demonstrates the need for 2 elements of a precise model: geometry and thermodynamics.

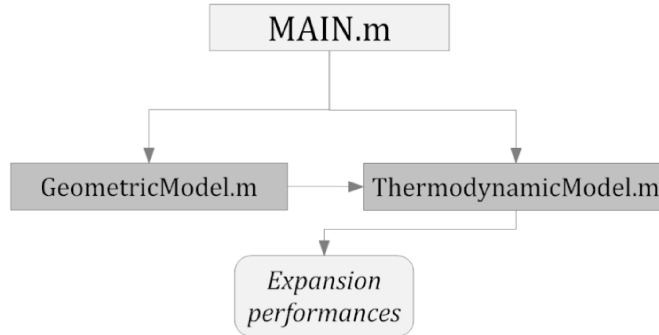


Figure 2.8: Lemort Model Architecture

The work of Ziviani et al. [28] was focused on the development of a detailed model of screw expander. Similarly to the work of Lemort, the model is based on both modeling the geometric intricacies of a screw expander, and then solving a set of differential equations to determine the thermodynamic performance of the expander. The model is based on a rotation-dependent function that entirely describes the geometry of the engaging surface between the screw rotor and the starwheels. The computation of the swept volume at each angular step and the inlet conditions enables the solution of the system of differential equations governing the thermodynamics. The model accounts for leakage, friction and simplified heat transfer relationships with special attention paid to how the geometry of the machine affects each parameter.

The work of Glavatskaya et al [29] developed a a model predicting the performance of a reciprocating piston expander in a similar fashion to the two works already mentioned. The work begins with an accurate geometric relationship of a piston expander including port surface area relationships. The geometric data is used as an input for the thermodynamic solver, and the performance of the device can be evaluated.

Stosic [50, 51] developed both a 1-D and 3-D model of a screw compressor and combined the two into a hybrid approach for calculating performance. The 1-D approach is used to generate in cylinder temperature and pressure conditions which are used as inputs in the 3-D model to calculate, for example, whether thermal expansion of the mechanical components can affect clearances and leakage. The goal of the hybrid approach was to minimize computational time while still providing insight into the trends that are caused by changes in operating conditions. The clear trend in the modeling work in this area thus far is the development of both accurate geometric relationships used as inputs into thermodynamic models.

3 Model Development

3.1 Simulation Goals

The goal of an automotive waste heat recovery system is to maximize the fuel savings obtained through the ORC. In order to do this, the selection of an expander type has been identified as one of the main areas concerning the optimization of the system. Proper selection of an expander type is not a simple task - there are many types of expanders available (piston, rotary vane, scroll, screw) and each has its own advantages and disadvantages. To add to the complexity, the type of working fluid, pressure ratio, flow rate, and rotational speed range are just a few of the other variables which can drastically affect expander performance [15], and therefore the overall cycle performance.

The first goal of this work is to provide a way to examine the performance of various expander types and geometries. The chosen approach is to develop a generic thermodynamic template for expander evaluation. In practise this means that the model will deal with the thermodynamic expansion process taking place in the expander in detail, while allowing a complex geometry to be entered as a function by the user.

In order to achieve a high level of accuracy with respect to a given expander type, accurate geometrical relationships which describe the change in working volume with time are required, along with thermodynamic models. Often these geometric relationships can be complex and vary from expander to expander - the geometry of a scroll expander is different than that of a screw or rotary vane expander. However, by allowing a user who is familiar with the geometry of a specific type of machine to specify the geometry, the thermodynamic aspect of the model can be developed with the geometrical characteristics as an input. In this way, a generic thermodynamic tool for expander performance and selection can be developed. The first application

of this model is in assisting in the design choices of an experimental test rig through error analysis.

The second goal of this work is to examine expander heat transfer through an analysis of the thermal behaviour of its mechanical components. Current modeling approaches often use an adiabatic assumption for expander modeling which assumes that performance losses due to heat transfer are negligible. A second application of this thesis is to verify the validity of this assumption, and to quantify the degree to which expander performance is affected by heat transfer losses. Similarly, most currently available models focus on expander operation at room temperature. A third application of this model is to examine expander performance under various ambient temperatures – especially in cold start situations where a vehicle can be started at temperatures lower than -20°C .

3.2 Simulation Approach

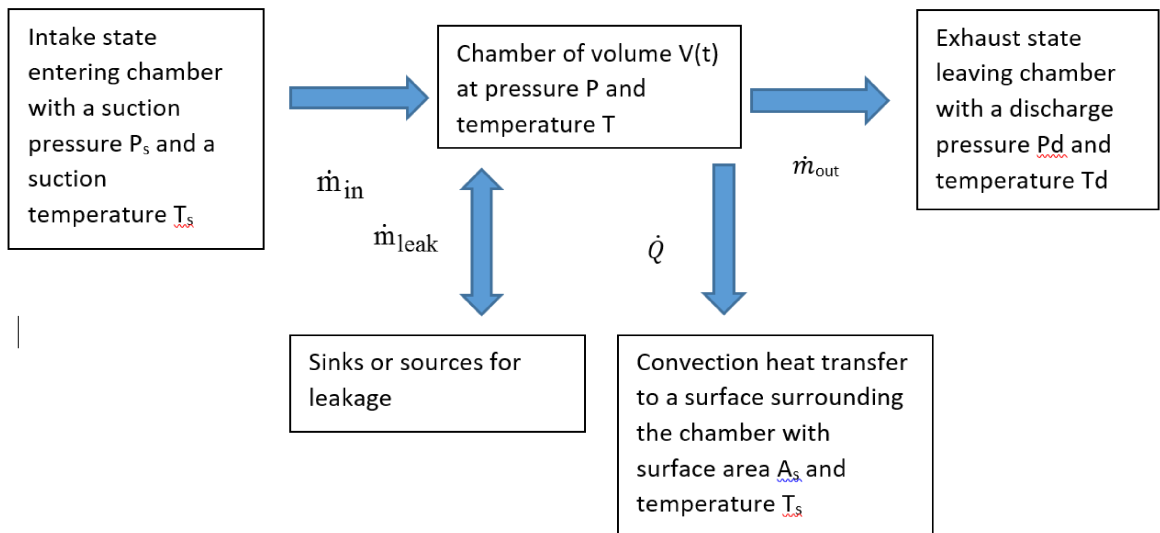


Figure 3.1: Model Setup

The model operates as a generic template which can be used as a thermodynamic tool for expander performance analysis as shown above in Figure 3.1. The main concept

is to develop a set of differential equations which can describe operating conditions inside an expander. By solving these equations over a number of revolutions of the machine, we can obtain the pressure and temperature in the working chamber and use them to calculate performance characteristics of the device.

The working principle is to develop a set of differential equations which are discretized into a number of time steps and solved numerically. The time step varies with the operating conditions and can often range from 1/1000th of a degree to 1/10th of a degree based on how demanding the operating conditions are. The time step is constant throughout the simulation is chosen by the user before the simulation begins, and is typically based on a trial and error approach which is estimated based on the severity of the initial operating conditions. This means that the 360 degrees of revolution which represent one crank cycle can be discretized into anywhere from 3600 steps to 360,000 steps. Consider that the model may run through anywhere from 1000 to 10,000 iterations of one full revolution (each with 3600 - 360,000 steps), and it becomes clear that the model can become computationally intensive.

As shown below in Figure 3.2 the working chamber is the working gas space - the volume where the expansion of gas actually takes place. It has a volume that changes with time (specified by the user) and is at some pressure P and temperature T throughout the expansion process. The intake conditions are assumed to be constant and are also model inputs - the intake temperature T_s and intake pressure P_s upstream of the expander. The exhaust state is also treated as a model input - the exhaust temperature T_d and exhaust pressure P_d downstream of the expander. There are also sources of leakage within the expander which contribute to mass leaving the working space where it is unable to expand, along with heat transfer paths for energy to leave the working space. By considering these factors and developing equations that represent the temperature and pressure inside the cylinder throughout the expansion process, the efficiency and power output of the device can be calculated.

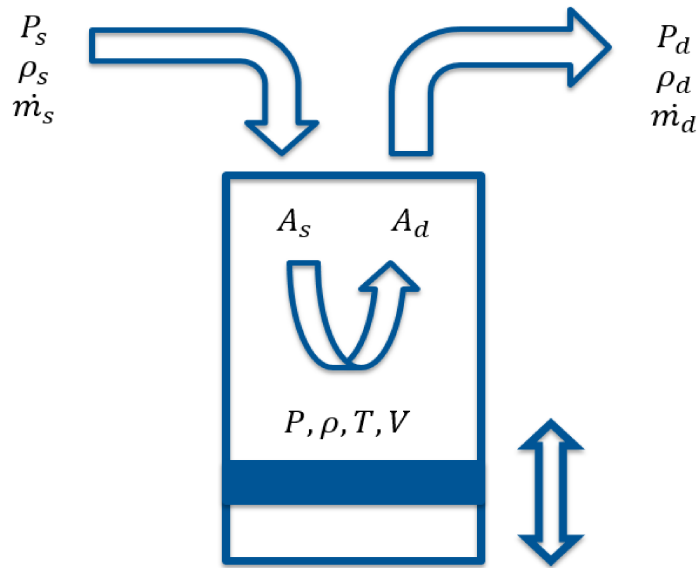


Figure 3.2: Generic Template

It is important to note that the model takes user inputs for a number of parameters. User inputs are required for geometric relationships, port surface areas, and heat transfer characteristics. Geometric relationships including the change of the working volume with time and the change of port surface area with time allow the user to differentiate between various types of expanders – a scroll expander will have different geometrical parameters than a screw or rotary vane expander.

The model also has the ability to evaluate the effects that heat transfer throughout the various mechanical components in the expander have on the working gas space. Many models that are currently available in literature [23, 24, 25, 26, 33, 5, 50] analyze the working gas space thermodynamics. Any heat transfer modeled in these works will be modeled as convective heat loss to a general ambient environment. This thesis takes into account heat transfer in all of the mechanical components found in a generic expander type. The significance of this is the ability to evaluate whether these components have a drastic effect on expander performance. Also, it allows for examination the a cold start on the expander - for example, the model can answer the question of what effects starting the vehicle in -20°C would have on the system.

This analysis is performed by examining the heat transfer through various lumped masses found in a generic expander. By solving a differential equation representing a heat transfer balance at each component, the temperatures of each component and their overall effect on the working gas space conditions can be calculated. There have been 7 different components identified as being present in all expander types and their effects are examined. Below in Figure 3.3 is a diagram which shows the 7 components of the heat transfer analysis:

1. Intake Enclosure
2. Exhaust Enclosure
3. Working Gas Space
4. Internal Mass (Piston, Rotor, Scroll, Screw)
5. Casing
6. Secondary Mass
7. Envelope around Secondary Mass

The diagram displays the geometry of a scroll expander as an example of what one can expect to see in a variety of different expander types. While the geometry of the working gas space may differ widely between expander types (the scroll pictured will be different than a screw geometry in the working gas space) the 7 components pictured should be present in almost all expander modern expander models.

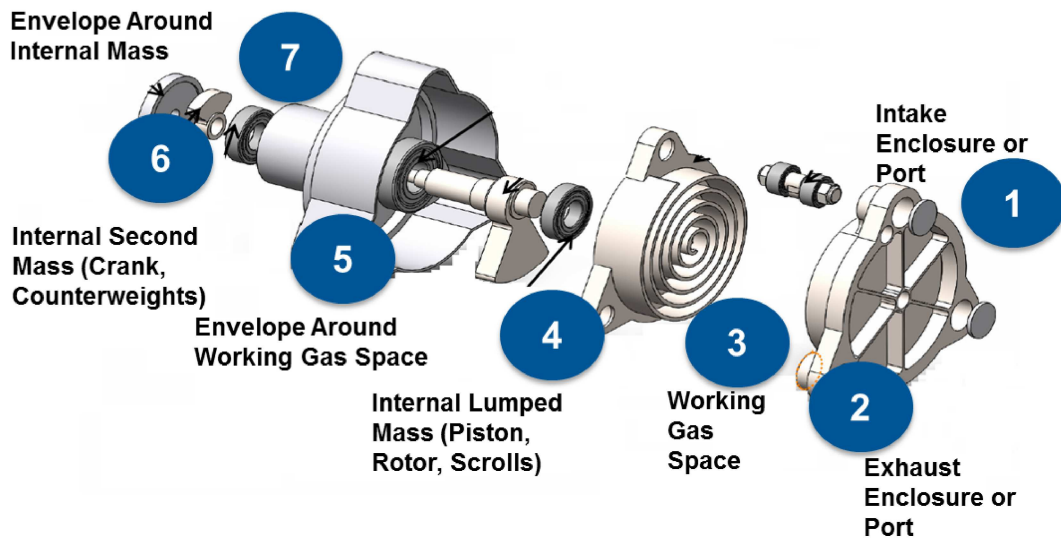


Figure 3.3: Heat Transfer Components Diagram

3.2.1 Model Assumptions

Assumptions made in the model include the following:

- Gaseous flow only – the fluid remains superheated vapour throughout the expansion process
- Ideal gas assumption – the model assumes that whichever fluid is used in the model is an ideal gas. This leads to the following:
 - Gas enthalpy is a function of temperature only
 - Ideal gas law can be used for calculating cylinder pressure
- Perfect gas assumption – the specific heats are constant and not a function of temperature
 - The specific heat value is the average value between the actual specific heats at inlet and outlet conditions
- Volume relationship is modeled with sin function – generally representative of a piston or rotary vane expander type

- Port surface area relationships are sin function representative of general expander conditions based on supplier data
- Frictional losses are modeled as through a mechanical efficiency factor
- All leakage flows from suction to discharge through only one uniform leakage path
- All gas in the cylinder is assumed to have uniform properties

3.3 Derivation of Governing Equations

A derivation of the governing equations which are used to calculate the performance of the expander is provided below:

3.3.1 Temperature and Pressure

The derivation begins by examining the principle of the conservation of mass:

$$\frac{dm}{dt} = \dot{m}_s - \dot{m}_d - \dot{m}_L \quad (3.1)$$

Where $m = \rho V$ and

\dot{m}_s represents the suction mass flow rate.

\dot{m}_d represents the discharge mass flow rate.

\dot{m}_L represents the leakage mass flow rate.

Conservation of energy for the control volume is given by:

$$\frac{dE}{dt} = \dot{m}_s h_s - \dot{m}_d h_d - \dot{m}_L h_d - P \frac{dV}{dt} - \dot{Q} \quad (3.2)$$

Where E is the total energy ($E = mu$), $P \frac{dV}{dt}$ is the mechanical work done by the system and \dot{Q} is the heat transfer from the system to the surroundings. The enthalpy terms represent the energy carried across the boundary by the fluid streams while

ignoring the contributions of kinetic and potential energy. For an ideal gas with constant specific heat, the following substitutions can be made:

$$u = C_v T \quad (3.3)$$

$$h = C_p T \quad (3.4)$$

$$P = \rho R T \quad (3.5)$$

So that the energy of the system becomes:

$$\frac{dE}{dt} = \frac{dm C_v T}{dt} = m C_v \frac{dT}{dt} + C_v T \frac{dm}{dt} = \dot{m}_s C_p T_{in} - (\dot{m}_d + \dot{m}_L) C_p T_{out} - P \frac{dV}{dt} - \dot{Q} \quad (3.6)$$

By substituting the expression for $\frac{dm}{dt}$ into 3.6 and rearranging the equation:

$$\frac{dT}{dt} = \frac{\dot{m}_s (C_p T_{in} - C_v T) - (\dot{m}_d + \dot{m}_L) (C_p T_{out} - C_v T) - \frac{P}{m C_v} \frac{dV}{dt} - \frac{\dot{Q}}{m C_v}}{m C_v} \quad (3.7)$$

In order to obtain temperature in relation to crank angle, substitute the relation between crank angle, angular velocity and time:

$$\theta = \omega t \quad (3.8)$$

And by taking the derivative and rearranging the equation:

$$dt = \frac{d\theta}{\omega} \quad (3.9)$$

Substituting this expression into equation 3.7 the first governing differential equa-

tion is obtained:

$$\frac{dT}{d\theta} = \frac{\dot{m}_s(C_p T_{in} - C_v T) - (\dot{m}_d + \dot{m}_L)(C_p T_{out} - C_v T)}{m C_v \omega} - \frac{P}{m C_v} \frac{dV}{d\theta} - \frac{Q}{m C_v \omega} \quad (3.10)$$

And by performing the same substitution on equation 3.1 the second governing equation is obtained:

$$\frac{dm}{d\theta} = \frac{\dot{m}_s - \dot{m}_d}{\omega} \quad (3.11)$$

Where the volume V of the chamber is determined by the following expression:

$$V = V_c + V_d \sin\left(\frac{\theta}{2}\right) \quad (3.12)$$

And the derivative of volume with respect to crank angle is given by the following expression:

$$\frac{dV}{d\theta} = 0.5 V_d \cos\left(\frac{\theta}{2}\right) \quad (3.13)$$

Where V_c is clearance volume, V_d is displaced volume, and θ is crank angle in radians.

Since the volume as a function of time is known, the density in the chamber can be computed:

$$\rho = \frac{m}{V} \quad (3.14)$$

The pressure can be calculated using the ideal gas equation:

$$P = \rho R T \quad (3.15)$$

3.3.2 Mass Flow Rate

A method for calculating mass flow rates is based on isentropic compressible fluid flow through a nozzle as described by Dikes[5] which includes separate equations for normal and choked flow as shown below:

$$\dot{m} = A\sqrt{(2P_s\rho_s)}\sqrt{\frac{k}{(k-1)}\left[\left(\frac{P}{P_s}\right)^{\frac{2}{k}} - \left(\frac{P}{P_s}\right)^{\frac{k+1}{k}}\right]} \text{ if } \frac{P}{P_s} < P_{crit} \quad (3.16)$$

$$\dot{m} = A\sqrt{(2P_s\rho_s)\frac{k}{(k+1)}\left(\frac{2k}{k+1}\right)^{\frac{1}{k-1}}} \text{ if } \frac{P}{P_s} > P_{crit} \quad (3.17)$$

$$P_{crit} = \left(\frac{2}{k+1}\right)^{\frac{k}{k-1}} \quad (3.18)$$

3.3.3 Efficiencies

The total amount of mass discharged through the machine in one cycle is:

$$m_{actual} = \int \dot{m}_s dt \quad (3.19)$$

The ideal amount of mass through the machine is the product of suction density and displacement volume:

$$m_{ideal} = \rho_s V_d \quad (3.20)$$

And volumetric efficiency can be calculated by comparing the two values:

$$\eta_v = \frac{m_{actual}}{m_{ideal}} \quad (3.21)$$

The work done by the expander during one cycle is given by:

$$W_{actual} = \eta_m \int PdV = \eta_m \int \frac{PdV}{dt} dt = \eta_m \int \frac{PdV}{d\theta} d\theta \quad (3.22)$$

The ideal (isentropic) work per cycle can be developed as follows:

$$W_{is} = \dot{m}C_p(T_{in} - T_{out}) \quad (3.23)$$

$$W_{is} = \dot{m}C_p T_{in} \left(1 - \frac{T_{out}}{T_{in}}\right) \quad (3.24)$$

$$\frac{T_{out}}{T_{in}} = \left(\frac{P_{out}}{P_{in}}\right)^{\frac{k-1}{k}} \quad (3.25)$$

$$W_{is} = \dot{m}C_p T_{in} \left(1 - \left(\frac{P_{out}}{P_{in}}\right)^{\frac{k-1}{k}}\right) \quad (3.26)$$

Isentropic efficiency can be calculated by comparing the two values:

$$\eta_{is} = \frac{W_{actual}}{W_{is}} \quad (3.27)$$

The amount of power produced by the expander can be calculated:

$$P_{exp} = \frac{W_{actual}}{t_{cycle}} = \frac{W_{actual}}{60 \cdot RPM} \quad (3.28)$$

The average discharge temperature can be computed by analyzing the work done over the cycle:

$$W_{actual} = \dot{m}C_p(T_s - T_{d,avg}) \quad (3.29)$$

$$T_{d,avg} = T_s - \frac{W_{actual}}{\dot{m}C_p} \quad (3.30)$$

3.3.4 Heat Transfer

Heat transfer across each mechanical component in a given expander type can be evaluated by examining a heat transfer balance across each component.

A heat transfer balance at the rotor can be formed as follows:

$$m_R C_{vR} \frac{dT_R}{dt} = \sum h_{conv} A_{rotor} (T - T_R) - C_R Q_f \quad (3.31)$$

Where m_R is the mass of the rotor in kg, C_{vR} is the specific heat of the rotor (aluminum) in J/kgK, T_R is rotor temperature, h_{conv} is the convection coefficient between the metal and fluid, Q_f is the heat generated due to friction at the rotor, C_R is a coefficient representing the percentage of friction heat entering the rotor, and A_{rotor} is the surface area exposed to convection during one time step.

W_f represents the work needed to overcome friction in a closed system and can be represented by:

$$Q_f = W_f = F_f d = \mu F_f d = \mu P A_s d \quad (3.32)$$

Where P is the cylinder pressure pushing on the piston over a surface area A_s and through a distance d .

The differential equation describing the heat transfer at this component can be solved by adding the total of all heat transfer during each time step over one complete revolution of the rotor and solving the resulting differential equation over one cycle.

A similar heat transfer balance can be calculated at the casing:

$$m_C C_{vC} \frac{dT_C}{dt} = \sum h_{conv} A_{casing,in} (T - T_C) - h_o A_{casing,out} (T_C - T_{amb}) - C_C Q_f \quad (3.33)$$

The heat transfer coefficient can be calculated by calculating Prandtl, Reynolds,

and Nusselt number for each condition as described in [28] :

$$Pr = \frac{C_p \mu}{k} \quad (3.34)$$

Where μ is dynamic viscosity of the fluid taken from [30] in kg/ms, Pr is the dimensionless Prandtl number, and k is the thermal conductivity of R245fa [31].

$$Re = \frac{\rho LU}{\mu} \quad (3.35)$$

$$U = \omega R \quad (3.36)$$

$$L = V^{\frac{1}{3}} \quad (3.37)$$

Where Re is the dimensionless Reynolds number, U is the mean machine speed in m/s which is assumed to be the mean fluid speed [32], and L is the characteristic length in m – which for a volumetric expander device is the third root of the volume[33].

$$Nu = c Re^\alpha Pr^{\frac{1}{3}} \quad (3.38)$$

Where Nu is the Nusselt number. The constants c and α are selected to be 0.023 and 0.8 respectively as found in literature through the work of Jang [52]. The convection coefficient can now be calculated through the definition of the Nusselt number:

$$h_{conv} = \frac{Nu k}{L} \quad (3.39)$$

The heat transfer balance equations for the remaining components are completed in the same manner by examining the modes of heat transfer between corresponding

components:

Internal Secondary Mass (cranks, counterweights, etc):

$$m_{m2}Cv_C \frac{dT_{m2}}{dt} = \sum -\frac{k_{cond}A_{casing}}{x_{casing}}(T_{m2} - T_C) - \frac{k_{cond}A_{rotor}}{x_{rotor}}(T_{m2} - T_R) \quad (3.40)$$

Envelope around Secondary Mass:

$$m_{E2}Cv_C \frac{dT_{E2}}{dt} = \sum -\frac{k_{cond}A_{m2}}{x_{casing}}(T_{E2} - T_{m2}) - h_oA_{E2}(T_{E2} - T_{amb}) \quad (3.41)$$

Intake Enclosure:

$$m_{in}Cv_C \frac{dT_{in}}{dt} = \sum -\frac{k_{cond}A_{port}}{x_{gasket}}(T_{in} - T_{casing}) - h_oA_{in}(T_{in} - T_{amb}) \quad (3.42)$$

Exhaust Enclosure:

$$m_{out}Cv_C \frac{dT_{out}}{dt} = \sum -\frac{k_{cond}A_{port}}{x_{gasket}}(T_{out} - T_{casing}) - h_oA_{out}(T_{out} - T_{amb}) \quad (3.43)$$

The equations presented provide the basis for the calculations needed to arrive at expressions for the isentropic efficiency and power output of a generic expander type. By also adding expressions describing the heat transfer between mechanical components in the expander, the effect that their respective temperatures have on expander performance can be evaluated.

3.4 Modeling Process

The modeling process is summarized in Figure 3.4 below and each of the 9 steps explained.

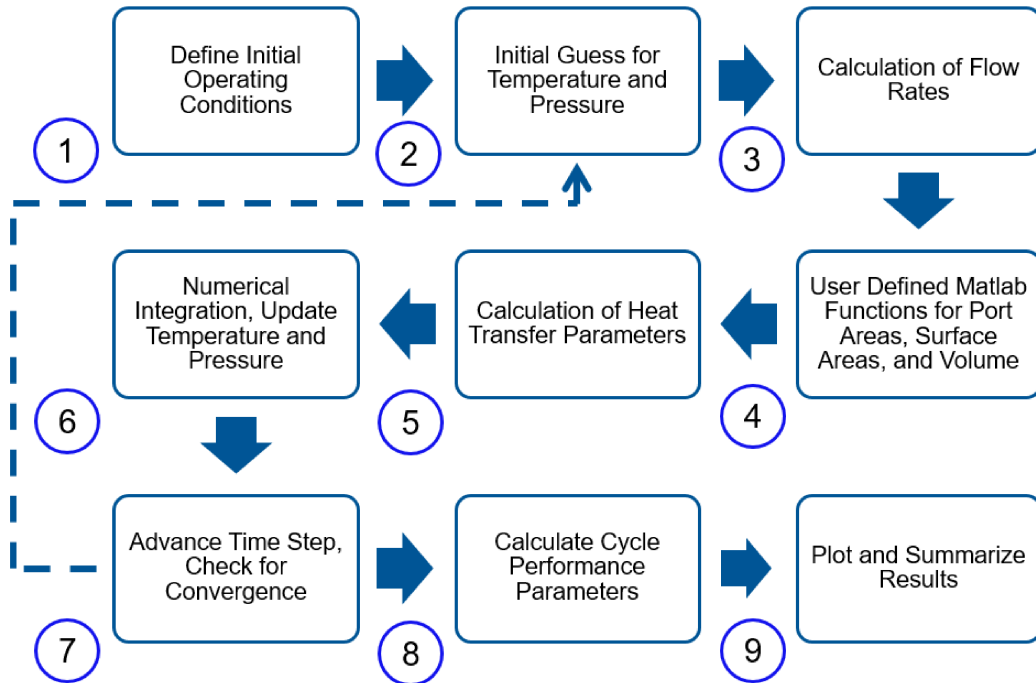


Figure 3.4: Process Flow Chart

3.4.1 Initial Operating Conditions

The process needed to arrive at a final result is an iterative process that must be repeated until the results converge. The model begins with the definition of the initial operating conditions. This includes the following variables:

- Upstream Conditions: Inlet Pressure, Inlet Temperature
- Downstream Conditions: Outlet Pressure, Outlet Temperature
- Gas Characteristics: Specific Heats, Gas Constant
- Expander Geometry: Working Chamber Volume and Port Surface Area Relationships

- Expander Operation: Clearance Volume, Displacement Volume, Rotational Speed
- Mechanical Components: Surface Areas, Masses, Heat Transfer Coefficients

3.4.2 Initial Guesses

Once the initial parameters pertaining to both the thermodynamic and physical conditions of the expander have been defined by the user, initial guesses are made by the user to supply the equations with a starting point for the calculations. If working correctly, the model will calculate the same final values regardless of the initial guesses given by the user. In fact, this is one way to check whether the model is running properly - no matter what the initial values are, the model should provide the same outputs and final performance calculations.

The following parameters require initial guesses and their values are calculated each iteration until convergence:

- Cylinder Temperature (T)
- Cylinder Pressure (P)
- Temperature of Mechanical Components (Rotor, Casing, Ports, Secondary Mass, Envelope)

3.4.3 User Defined Functions (Volume, Port Surface Area)

Once the initial guesses and input parameters are entered into the model, there are a number of important parameters which must be entered by the user in order to run the model properly.

Volume

Since the performance of the expander is linked to the geometry of the machine in question, the volume relationships are an important element of the model development. The chosen equation describing the volume evolution in the chamber is based on a sin function which is representative of the volume changes that can be found in a piston type expander[33] or a rotary vane[34] type expander. In both of these devices, the volume goes from the clearance volume (minimum) to the maximum volume in a sinusoidal movement in a function such as:

$$V = V_c + V_d \sin\left(\frac{\theta}{2}\right) \quad (3.44)$$

which represents a sin function with a period of 360 degrees, or one full revolution of the machine and is depicted below in Figure 3.5.

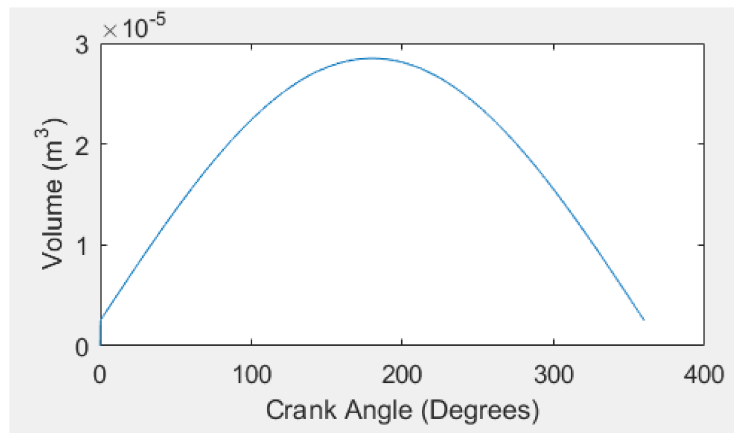


Figure 3.5: Gas Space Volume Relationship

It is important to note that while this geometrical function is generally representative of the gas space evolution of a piston and rotary vane type expander, the geometry of a scroll and screw type expander is more complex. These devices contain mating parts that create many different pockets of fluid within the expansion chamber, each with their own geometric relationship which describes the gas volume in

that specific chamber. As described below, a modular approach is used which allows the user to input customized volume relationships which allow differentiation between various expander types. For the purposes of the development of the model, equation 3.44 which is depicted in Figure 3.5 was chosen as the volume relationship used for all of the calculations.

Port Surface Areas

Port surface areas are another consideration when developing a model of an expander. Inlet and outlet port surface areas have a major impact on the amount of flow that can flow into and out of the expander. By modifying the value, duration and timing of the inlet and outlet ports, the performance of the expander can be affected. However, the port surface area relationships will differ greatly between expander types.

To emphasize this, consider that a piston and rotary vane expander use valves to control the precise timing and duration of the inlet and outlet processes, while the flows in a scroll and screw expander are imposed by the conditions inside the expander (they are self-regulating). Furthermore, a scroll expander may have blockages created in the inlet flow path due to scroll tip interference. These intricacies are specific to each form of expander and are difficult to capture in a generic expander model. However, Brummer [35] and Lemort [6] showed that port surface areas can be relatively well approximated using sin functions for inlet and outlet as follows:

$$A_{port} = B \sin(C\theta) \quad (3.45)$$

Where B is a factor corresponding to the magnitude of the port opening, and C is a factor corresponding to the duration of the port opening.

The equations used in the model are:

Inlet Port

$$A_{in} = 0.0005 \sin\left(\frac{180}{\theta_{cutoff,in}}\theta\right) \quad (3.46)$$

Outlet Port

$$A_{out} = 0.001 \sin\left(\frac{180}{\theta_{cutoff,out}}\theta\right) \quad (3.47)$$

Figure 3.6 below depicts the port surface area relationships for a single case in the simulation. The suction port is open from 0-30°CA to a maximum area of $0.0005m^2$ ($5cm^2$). The discharge port is open from 180-360°CA to a maximum area of $0.001m^2$ ($10cm^2$). Typically, the discharge port of an expander is larger than the inlet port and is open longer to allow the low pressure gas to fully escape from the expansion chamber before the process is complete.

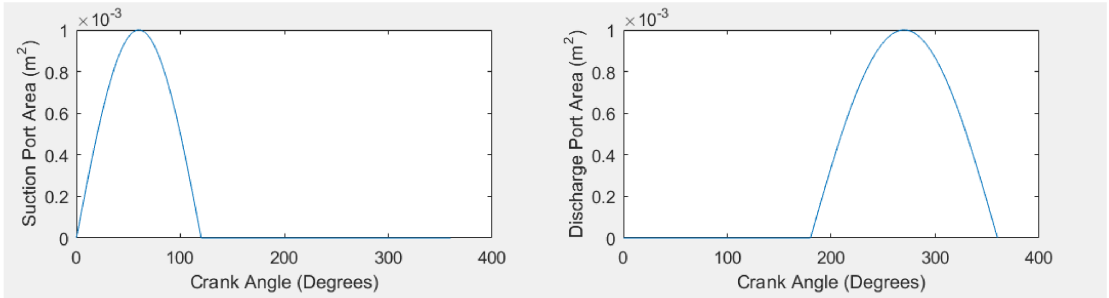


Figure 3.6: Port Surface Areas

Theoretically, there are an unlimited number of possible relationships describing port surface areas. However, as the goal of the thesis is to focus on and develop a generic thermodynamic tool without precise considerations of geometry particular to one type of device, one standard set of port surface area equations was chosen for comparison and analysis. The equations shown were chosen on the basis of being a reasonable estimate of port surface area relationships found in literature [35, 6, 17] and deemed generally capable of representing reality.

Modular Approach

The modular approach used in this model allows the user to substitute elements of the model with their own functions. The user has control of the volume of the chamber, port surface areas and lumped mass areas and their masses. Functions are used to call these aspects of the code within Matlab, so the respective elements can be modified through a new function or change to the current function code. Generic values have been chosen for each modifiable parameter which are generally representative of expander operation as described previously.

An example of the user-defined functions for port surface areas and volume can be seen below in Figure 3.7. The user can input their own relationships into these functions to fit different expander types and geometries. Some geometrical relationships can be more complex and may require multiple lines of code to describe the complete geometry correctly. Lumped mass areas and masses can be modified within the code by simply changing the constant value before running the simulation.

```
function [Suc_Port_Area,Dis_Port_Area] = Port_Area(Inlet_Cutoff_Angle,Outlet_Cutoff_Angle,theta)
% This function calculates the port surface areas for the opening and
% closing of inlet (suction) and outlet (discharge) ports of an expander.
Suc_Port_Area = 0.0005*sin(180/Inlet_Cutoff_Angle.*theta.*pi()./180);
Dis_Port_Area = 0.001*sin(180/Outlet_Cutoff_Angle.*theta.*pi()./180);
end
```

(a) Port Surface Area Function

```
function [Volume,dVdTheta] = Vol_Func(Vc,Vd,theta)
% This function calculates the volume and change of volume with respect to
% time for a certain expander type. The current setup is for a piston or
% rotary vane type machine.
Volume = (Vc + Vd.*(sin(0.5.*(theta.*(pi()/180)))));
dVdTheta = 0.5.*Vd.*(cos(0.5.*(theta.*(pi()/180)))));
end
```

(b) Volume Function

Figure 3.7: Modifiable Function

Mass and Component Surface Areas

An important element of calculating heat transfer characteristics between the various components in the expander is their physical characteristics. In particular, the mass and surface areas of the components in question play a large part in their behaviour with respect to heat transfer. The ability to change the masses and surface areas of the mechanical parts is what allows the user to differentiate between the various geometries of parts that can be found in a variety of expander types. This means that the user must specify the size and mass of each component being analyzed in order to properly simulate its effects on the working gas space temperature and ultimately the performance of the machine. Therefore, the masses and surface areas of the 6 components must be specified: intake enclosure, exhaust enclosure, rotor, casing, secondary mass, envelope. Generic sizes and masses have been chosen according to supplier data and are summarized later in the report.

3.4.4 Flow Rates

Once the initial guesses are made, the mass flow rates can be calculated on the basis of the initial parameters defined by the user, along with initial guesses for temperature and pressure through the equations given above. The mass flow rates are based on isentropic compressible fluid flow through a nozzle as described by Dickes [5] and account for regular and choked flow conditions.

It is important to note that these mass flow rate calculations are based on the upstream and downstream pressure conditions in the expander. As the pressure evolves inside the cylinder, the amount of flow is mainly dependent on the pressure difference between the cylinder and the inlet/outlet ports. This results in mass flow rates that can vary substantially throughout the crank cycle of the machine. However, in real world testing, the mass flow rate through the expander is imposed by the pump. Therefore, the mass flow rates obtained and reported through tests is constant or very

nearly constant. This is a fundamental difference between the way tests are typically run and the way that the model treats mass flow rates.

3.4.5 Heat Transfer Parameters

After the calculation of flow rates, heat transfer parameters such as the Prandtl, Nusselt, and Reynolds number can be computed in order to calculate the convective heat transfer coefficient. Once the heat transfer coefficient has been calculated for that iteration, differential equations for each of the 6 components can be calculated at each time step through the method described above in Section 3.3.4.

3.4.6 Numerical Integration

Once all the preliminary calculations are complete (volume, port surface area, mass flow rate, heat transfer coefficient), the governing differential equations describing the temperature and pressure in the cylinder can be solved numerically. An Euler method solver is chosen for simplicity, ease of implementation in Matlab, and the ability to accurately control the time step. It can be described as follows [36]:

For an initial value problem with ODE in the form:

$$\frac{dy}{dx} = f(x, y) \quad (3.48)$$

$$y(x_o) = y_o \quad (3.49)$$

The Euler method can be expressed as:

$$x_{n+1} = x_n + h \quad (3.50)$$

$$y_{n+1} = y_n + hf(x_n, y_n) \quad (3.51)$$

So that within the code, the Euler method solution appears as:

$$T_{new} = T_{old} + \frac{dT}{d\theta}d\theta \quad (3.52)$$

$$m_{new} = m_{old} + \frac{dm}{d\theta}d\theta \quad (3.53)$$

One part of this code (Mass and Temperature) are solved and recalculated every time step, while the heat transfer parameters are recalculated after one full revolution of the machine.

This same technique is used to solve for the temperatures of each of the 6 lumped masses, but instead of integrating and solving every time step, they are recalculated after each full iteration, or after each 360 degree revolution of the machine. Therefore, the heat transfer which is calculated at each time stepped is summed up for all 360 degrees of that crank cycle and then integrated with respect to the entire cycle. The reason for this is that heat flows are very small for the small time steps that are needed to solve the set of differential equations, so the entire sum of those heat flows can be updated once every revolution. The expression for the component temperatures (rotor shown below) is similar to the equations above and is solved in the same way, but less frequently:

$$T_{Rotor,new} = T_{Rotor,old} + \frac{dT_{rotor}}{d\theta}d\theta \quad (3.54)$$

3.4.7 Convergence Check

At the beginning of the code, the initial guesses are used as a starting point for the calculation of variables. Once all the necessary parameters are calculated based on these initial guesses, the differential equations are solved and each of the variables are updated as their new calculated value. The time step is advanced, and the process

begins again at the new time step. In this way, the code runs through the first 360 degrees of rotation of the machine and obtains a time history of the cylinder conditions.

Next, the code begins calculating the next rotation of the machine. The last values obtained are used as initial guesses, and in this way the code corrects itself and the values become more and more accurate with each iteration. In order to properly identify when the model has achieved satisfactory results and the simulation is complete, a criteria must be set for deciding on the convergence of the results. Deciding on convergence can be done in two ways. The first is by manually selecting a number of revolutions of the machine and observing the plots to see when the heat transfer through components is equal to zero. The second method is to set an automatic stop to the code once the temperature difference between the last two calculated iterations is small enough. This is usually done when the rotor or casing temperature reaches about 0.01 degrees C between revolutions to achieve adequate steady state conditions.

3.4.8 Performance

Once convergence has been reached and the final data set has been obtained, those values can be used to calculate the final goal of the model - the performance parameters. Isentropic efficiency can be calculated on the basis of comparing the calculated P-V work done on the piston to the theoretical amount that should be produced. The actual work can be divided by the time of the cycle to calculate the power produced by the expander. The volumetric efficiency can be calculated by comparing the actual amount of mass taken in to the maximum theoretical mass that can be held inside the expander. The results are reported and summarized in a table.

3.4.9 Results Summary

Once convergence has been reached, the final obtained data set can be plotted and analyzed. The following parameters can be plotted:

- Cylinder Pressure vs. Crank Angle
- Cylinder Temperature vs. Crank Angle
- Cylinder Gas Density vs. Crank Angle
- Suction/Discharge Mass Flow Rate vs. Crank Angle
- Cylinder Pressure vs. Volume (P-V Diagram)

4 Results

4.1 Modeling Objectives

There are 3 main goals of the simulation work:

1. Provide the ability to examine the performance of different expander types and geometries
 - A generic, modular approach is chosen to give the user the ability to differentiate between expander types through customizable functions
2. Examine expander heat transfer through an analysis of the thermal behaviour of its mechanical components
 - A heat transfer balance is performed at each mechanical component to examine its respective effect on the thermal behaviour of the device
3. Create a detailed physics-based model to be used as a benchmark for simpler models
 - The generic simulation tool is used as a detailed tool to calibrate simpler models which are not examined in this thesis

Within the framework of the 3 main goals of the thesis, there are 3 main applications (Part A, B, C) which demonstrate the applicability of the model to solve the outlined thesis goals. The results section will examine the following applications in detail:

1. Assist in the analysis of experimental testing techniques
 - (a) Testing results used in this thesis were obtained in late 2014 and early 2015. After analyzing the results of the testing, there are a few areas which require specific explanation. Numerical calculation of the isentropic

efficiency for certain testing points reveals a high sensitivity to the discharge temperature of the expander. The thermocouple selected for the discharge temperature measurement contains an error of $\pm 2.2^{\circ}\text{C}$. However, even within this tolerance, that can lead to considerable errors in power in excess of 20%. Such errors are considered high enough to become problematic when also considering that errors associated with other measurement devices such as pressure transducers and other DAQ equipment can also considerably add to the overall isentropic efficiency error.

- (b) For this reason, an alternate approach was adopted for the use of the model. The idea is to first calculate the sensitivity of the overall shaft power output to changes in expander discharge temperature using NIST equations, and then to perform a similar analysis using the model. In this way, the model can be used as an experimental design tool which could show the acceptable limits of error for temperature readings.
2. Determine the validity of the adiabatic expander assumption used ORC system models
 - (a) ORC system level models often employ simplified 0-D models for the expander with the objective of lowering computational time for simulations. Such a model uses an adiabatic assumption for the expander, and ignores the contribution that heat transfer from the working chamber has on expander performance. An important objective of this work is to test whether this assumption is acceptable.
 3. Examine effects of ambient temperature on expander performance
 - (a) Current models available in literature focus on expander testing and modeling at ambient conditions, where most expanders and ORC systems will operate. However, of interest in automotive applications is the effect of a

cold start (starting the system at very cold conditions) on the performance of the system. For example, it is logical to assume that the system would operate differently when exposed to an environment at -20 degrees C than when exposed to an ambient temperature of +20 degrees C. The ability to analyze heat transfer contributions in this model will allow the effects of a cold start on performance to be quantified.

- (b) Similarly, the model allows the user to see how long it takes for the expander to reach its full operating potential. This could provide valuable insight on when to actually engage the system on a real vehicle - it may only be valuable when the system is at its peak efficiency.
- (c) The thermal time constant of the expander is important for the design of a control system for ORC testing. The model can calculate the thermal time constant of the expander under various ambient temperature simulation conditions.

4.2 Experimental Testing Setup

Testing was performed on an Organic Rankine Cycle rig which was designed for automotive specific testing. The testing was carried out before work of this thesis, but the author was not involved in the testing procedures.

The test rig contains the 4 main components of an Organic Rankine Cycle: a dedicated pump, evaporator, expander and condenser, and also adds a recuperator to preheat/precool the fluid before it enters the evaporator and condenser respectively. For automotive applications, the engine exhaust heat acts as the evaporator of the working fluid through a closed loop heat exchanger with an intermediate fluid. The characteristics of the fluid upstream of the expander are modified by changing engine operating parameters. Another closed loop circuit is connected to the condenser, where coolant is used as the intermediate fluid to condense the vapour back into a

liquid.

The goal of the testing was to characterize the expander by developing performance plots of the isentropic efficiency and power output as a function of the pressure ratio at different operating speeds (similar to the above diagrams and procedure). The testing was performed for steady state conditions.

Figure 4.1 displays the setup of the ORC system including all measurement devices.

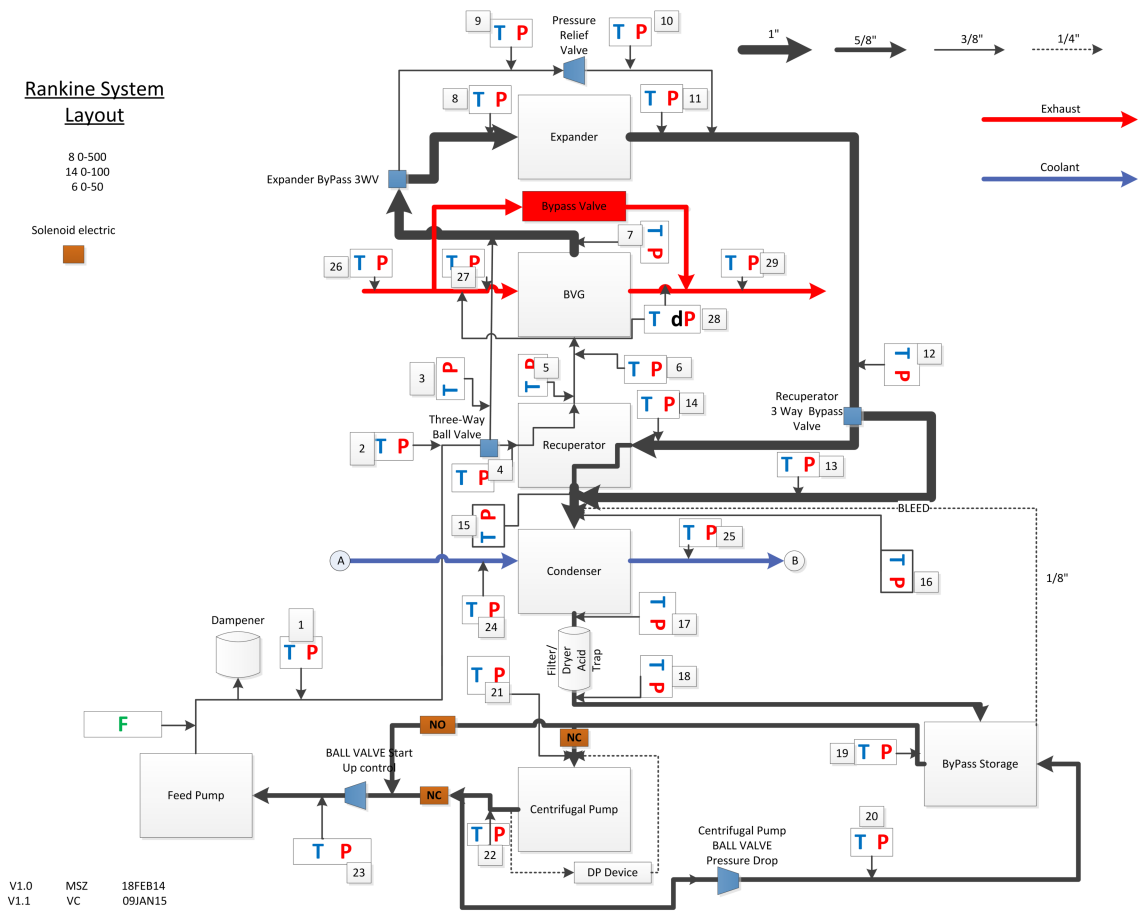


Figure 4.1: ORC Test Setup Diagram

The following measurement devices are relevant in the testing of the expander:

- Thermocouples[54]
 - Omega K-Type Nickel-Chromium

- Grade: 200 - 1250^oC
- Limits of Error: 2.2^oC or 0.75% Above 0^oC
- Pressure Transducers[55]
 - GE UNIK 5000 Silicon Piezoresistive Pressure Sensor
 - Grade: 70 mbar to 700 bar
 - Limits of Error: $\pm 0.04\%$ Full Scale (FS) Best Straight Line (BSL)

4.3 Experimental Testing Procedure

An important part of the testing is the need to keep the inlet conditions and mass flow rate as constant as possible throughout the operating points in order to isolate the effects of pressure ratio on performance. The idea is to run through a sweep of various pressure ratios ranging from 2 to 7 for each expander rotational speed. The pressure ratios are not necessarily set points and therefore are not standardized and the same for each speed, but generally there should be a balance of speeds in the same range for each speed.

The pressure ratio is modified by changing both the high side and low side pressure of the expander. The low side pressures can be modified by controlling the coolant flow rate. To modify the high side pressure, the heat input into the cycle is modified by changing the engine speed, load and spark advance.

A goal is to keep the temperatures at the expander inlet constant with respect to the other testing points in that batch. While the inlet conditions between different tests at varying speeds do not necessarily have to be the same, the suction temperature between operating points at the same speed should be fairly constant and could range from 150-200^oC depending on the chosen conditions.

The tests start at 1000 RPM and results are recorded for each 500 RPM increment after that, up to 3500 RPM. 1000 RPM is chosen as a starting point as the very

minimum expander speed at which an ORC system will ever run, but often this speed is never used or reached because the system efficiency is low at such a low speed range. 3500 RPM is chosen as the upper limit because it is suggested as the maximum safe operating speed of the expander by the supplier. The 2500 RPM speed is neglected because it is a resonance frequency of the machine, and causes high NVH which could potentially damage other system components near it.

The expander RPM and initial pressure ratio is chosen and the system is allowed to reach steady state conditions. Throughout the testing procedure, steady state conditions are assumed to be reached when expander inlet temperatures vary less than 1 degree C per minute and when pressures vary less than 0.05 bar per minute at the judgement of the testing engineer. Once steady state is reached for each operating point, 20 seconds of recording is done at each interval with 1 recording performed each second, with the last 6 seconds recorded averaged and compiled in a database of results. The pressure ratio is then modified through controlling the high and low side pressure of the system. The sweep continues in this manner until a satisfactory amount of pressure ratios has been tested. The RPM is then increased to the next desired speed, and the test is complete once all rotational speeds have been examined.

4.4 Part A - Analysis of Experimental Error

4.4.1 Note about Testing Results and Approach

As mentioned previously, the output power calculated based on experimental values obtained through testing has a high sensitivity to temperature readings at the exit of the expander. When considering the errors that can be carried through each sensor affecting the final result of isentropic efficiency, the total error can reach over 20% and can lead to unreasonable values of isentropic efficiency. In order to compensate for this, an alternate approach was considered, where the model is used as a tool to

evaluate the system sensitivity to downstream temperature readings to assist in the design of an experimental test.

4.4.2 Error Calculation Procedure

An error analysis is performed on experimental obtained through testing. An excel spreadsheet is used for the following calculations. The equations used for the calculation of each parameter are based on the NIST equations of state and can be found in the appendix.

1. Measure the work output of the expander on a dynamometer.
2. Calculate the inlet conditions from NIST equations based on temperature and pressure readings at inlet of expander.
3. Divide the measured shaft power by the mass flow rate to find the enthalpy change over the expander.
4. Subtract this from the inlet enthalpy to find the enthalpy at expander exit.
5. Calculate what the superheat would have to be to obtain this enthalpy.
6. Calculate the shaft power that would be obtained with two different superheat temperatures: +1 degree C and -1 degree C from the calculated theoretical superheat.
7. Subtract the upper and lower bounds of shaft work from the measured shaft work to find the amount of error caused by a 1 degree change in outlet temperature.
8. Divide the shaft error by the measured shaft power to find the percent error in shaft output power per degree Celsius change in measured outlet temperature.

A similar analysis is performed using the model to replicate the error calculation:

1. Measured input values from testing are used as fixed values for RPM, inlet temperature and pressure, and outlet pressure.
2. The model is run under given conditions.
3. The average discharge temperature is calculated as an output of the model.
4. The calculated discharge temperature is modified by +1 degree C and -1 degree C.
5. The work done as a result of modifying the discharge temperature is calculated.
6. The percent error in shaft power per degree change in discharge gas temperature is calculated.

4.4.3 Calculated Results

A summary of the conditions tested and simulated along with the calculation results is provided below in Table 4.1.

| | RPM | Power (W) | Pressure Ratio | Power +1°C (W) | Power -1°C (W) | Error Per °C (%) | Model Error Per °C (%) |
|----|------|-----------|----------------|----------------|----------------|------------------|------------------------|
| 1 | 1000 | 454.830 | 3.552 | 421.135 | 488.5 | 7.405 | 4.100 |
| 2 | 1000 | 579.258 | 4.260 | 542.011 | 616.5 | 6.427 | 3.740 |
| 3 | 1000 | 522.524 | 4.962 | 488.731 | 556.3 | 6.464 | 3.580 |
| 4 | 1000 | 628.243 | 5.741 | 591.044 | 665.4 | 5.918 | 3.460 |
| 5 | 1000 | 636.539 | 6.101 | 599.368 | 673.7 | 5.836 | 3.410 |
| 6 | 1000 | 625.684 | 7.098 | 591.518 | 659.8 | 5.457 | 3.190 |
| 7 | 1500 | 245.702 | 3.508 | 229.955 | 261.4 | 6.404 | 4.350 |
| 8 | 1500 | 675.720 | 4.119 | 636.774 | 714.6 | 5.761 | 3.780 |
| 9 | 1500 | 715.602 | 4.871 | 678.400 | 752.8 | 5.196 | 3.560 |
| 10 | 1500 | 743.104 | 5.527 | 705.944 | 780.2 | 4.998 | 3.460 |
| 11 | 1500 | 764.699 | 6.266 | 728.579 | 800.8 | 4.721 | 3.280 |
| 12 | 1500 | 781.613 | 7.523 | 745.793 | 817.4 | 4.580 | 3.190 |
| 13 | 2000 | 789.510 | 3.545 | 743.089 | 835.9 | 5.878 | 4.050 |
| 14 | 2000 | 740.447 | 4.251 | 701.247 | 779.6 | 5.291 | 3.720 |
| 15 | 2000 | 1258.418 | 4.696 | 1188.466 | 1328.318 | 5.557 | 3.630 |
| 16 | 2000 | 799.211 | 5.240 | 760.503 | 837.872 | 4.840 | 3.540 |
| 17 | 2000 | 1317.399 | 6.033 | 1247.825 | 1386.904 | 5.279 | 3.450 |
| 18 | 2000 | 774.553 | 6.828 | 741.720 | 807.339 | 4.236 | 3.340 |
| 19 | 2000 | 990.000 | 7.785 | 946.446 | 1033.493 | 4.396 | 3.300 |
| 20 | 3000 | 665.133 | 3.545 | 624.883 | 705.342 | 6.048 | 4.270 |
| 21 | 3000 | 1336.527 | 4.380 | 1268.541 | 1404.460 | 5.085 | 3.770 |
| 22 | 3000 | 1421.163 | 5.022 | 1353.317 | 1488.945 | 4.772 | 3.600 |
| 23 | 3000 | 950.000 | 5.805 | 910.330 | 989.621 | 4.173 | 3.190 |
| 24 | 3000 | 650.000 | 6.301 | 624.943 | 675.020 | 3.852 | 3.280 |
| 25 | 3000 | 824.530 | 6.974 | 791.820 | 857.193 | 3.964 | 3.310 |
| 26 | 3000 | 900.000 | 7.767 | 867.610 | 932.345 | 3.596 | 3.040 |
| 27 | 3500 | 558.502 | 3.181 | 520.310 | 596.659 | 6.835 | 4.270 |
| 28 | 3500 | 885.862 | 3.502 | 831.840 | 939.841 | 6.096 | 4.200 |
| 29 | 3500 | 610.698 | 4.013 | 577.253 | 644.103 | 5.473 | 3.840 |
| 30 | 3500 | 673.095 | 4.524 | 639.733 | 706.413 | 4.953 | 3.670 |
| 31 | 3500 | 805.796 | 4.973 | 768.295 | 843.249 | 4.651 | 3.550 |
| 32 | 3500 | 850.600 | 5.576 | 813.279 | 887.872 | 4.385 | 3.420 |
| 33 | 3500 | 762.014 | 6.191 | 729.149 | 794.832 | 4.310 | 3.410 |
| 34 | 3500 | 788.474 | 6.741 | 755.723 | 821.176 | 4.151 | 3.350 |

Table 4.1: Summary of Testing and Calculations

4.4.4 Plots

The data points are plotted below in for each of the 5 expander speeds tested. A discussion of the results is provided below the figures.

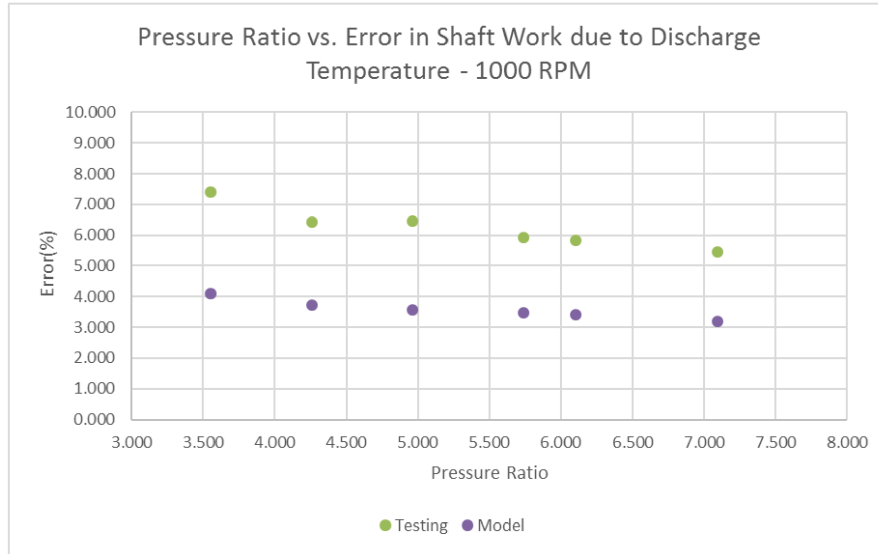


Figure 4.2: Error Analysis 1000 RPM

Figure 4.2 displays the sensitivity in shaft work as a function of pressure ratio for the 1000 RPM operating speed. The trend is almost linear and decreases with increasing pressure ratio. The error is slightly higher than the other speeds in this case due to inconsistent and inefficient expander operation at this speed range.

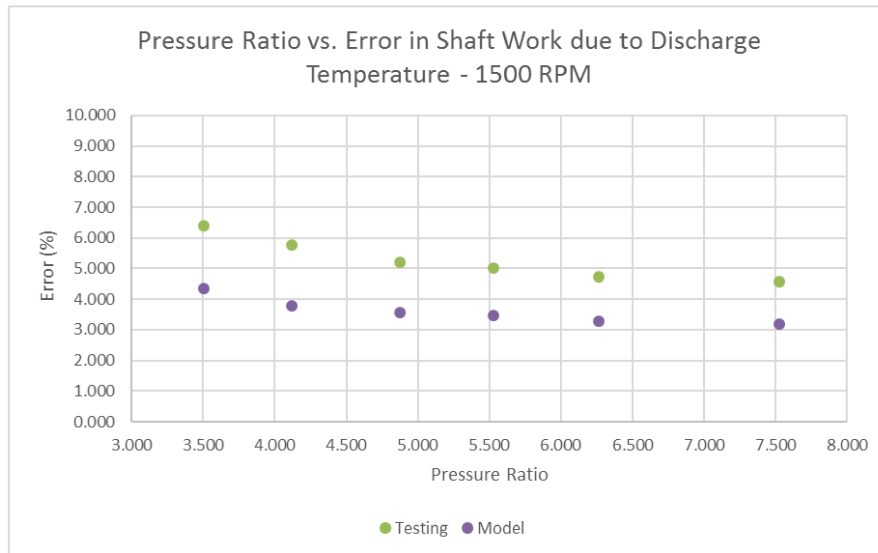


Figure 4.3: Error Analysis 1500 RPM

Figure 4.3 displays the results for an expander speed of 1500 RPM. Similar to

the previous case, nearly linear decrease in shaft error per degree change in discharge temperature is seen with increasing pressure ratio. Errors are slightly smaller than the 1000 RPM case as the expander operates more steadily at this speed.

Figures 4.4, 4.5 and 4.6 show the results for the last 3 operating speeds: 2000, 3000, and 3500 RPM. The 2500 RPM speed was not tested due to considerable NVH caused by a resonance frequency of operation. The remaining plots show a similar trend - decreasing error with increasing pressure ratio, and slight decreases in error with increasing speed. A discussion of results is provided below.

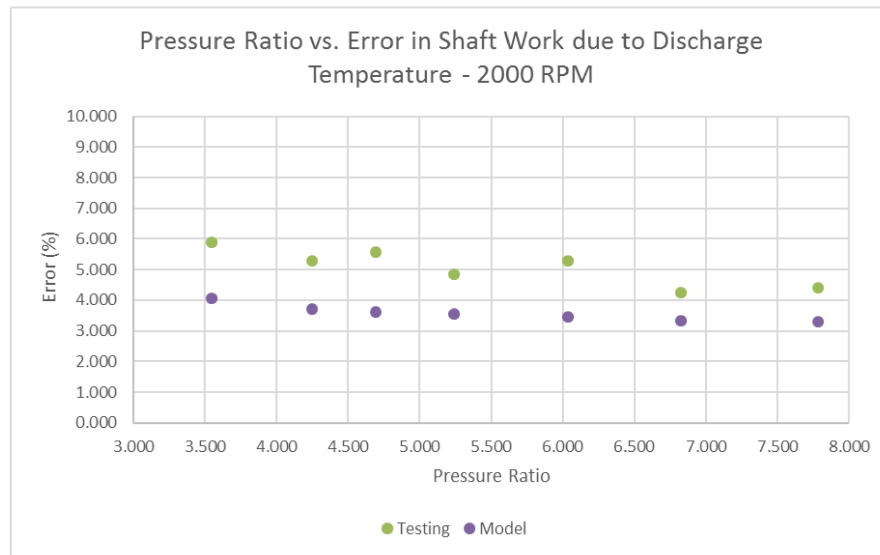


Figure 4.4: Error Analysis 2000 RPM

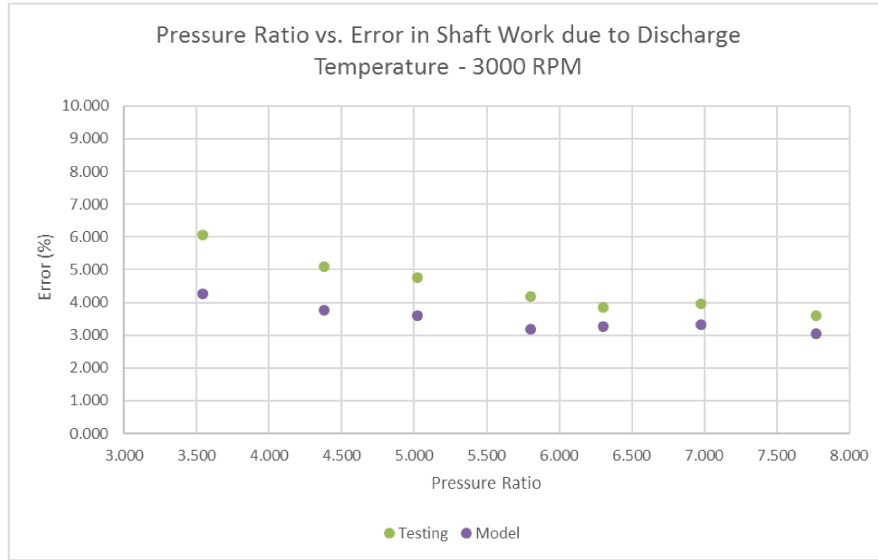


Figure 4.5: Error Analysis 3000 RPM

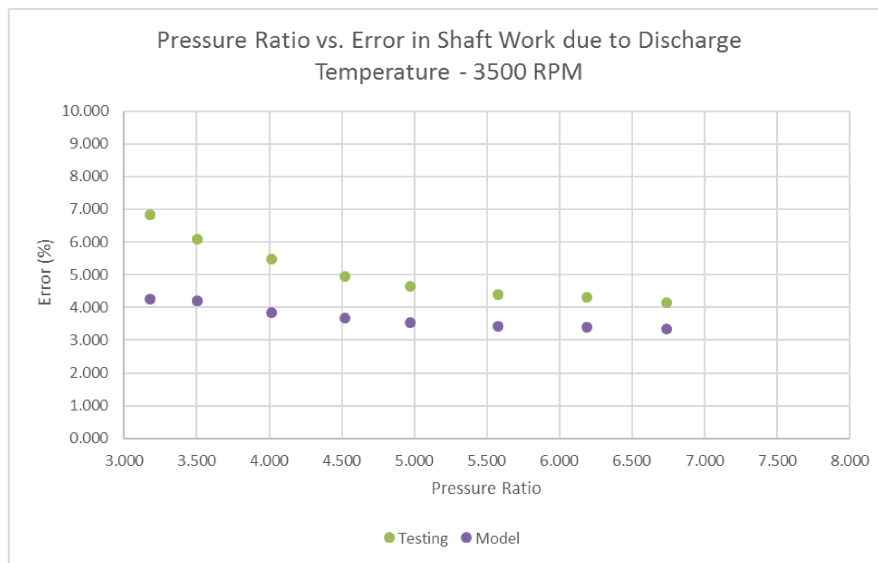


Figure 4.6: Error Analysis 3500 RPM

4.4.5 Discussion

From the plots shown above it is visible that the trend is for the error in shaft work per degree change in discharge temperature to decrease with increasing pressure ratio. This trend is evident for all tested expander speeds. The trend is generally irrespective of the design pressure ratio point of the expander, suggesting that under and over

expansion losses do not affect the sensitivity of temperature measurements.

The reason for this trend is the generally increasing expander efficiency at higher pressure ratios. While theoretically operation at lower pressure ratios (under 4-4.5) should be smooth, in practise low pressure ratios cause problems during testing as described by the testing engineer for the ORC system in this case. At low pressure ratios expanders are rarely run in practice as leakage losses during operation in this range are substantial, and the expander often cannot maintain steady operation at low pressure ratios, especially when run at lower RPM (under 2000). The relationship between shaft power sensitivity to downstream temperature is convoluted, but generally decreasing leakage losses and smoother expander operation at higher pressure ratios cause a smaller shaft power sensitivity to downstream temperature readings.

As can be seen in the results, the model consistently underestimates the error caused by changes in discharge temperature. The reason for this is the fact that the model predicts an idealized version of the expansion process which is free of “real world” problems which contribute to unpredictable expander behaviour - factors such as broken seals due to frequent expander use or poor maintenance or excessive friction or leakage due to poor design. Both of these issues were experienced throughout testing as described by the testing engineer responsible for this data.

The average error in shaft work per degree in discharge temperature calculated through NIST equations is 5.18%, and the error calculated by the model is 3.55%. With an error tolerance of $\pm 2.2^{\circ}\text{C}$ for the current thermocouple that was selected, errors in shaft power can reach in excess of 20%. Errors of this magnitude can discredit results obtained during testing, so a thermocouple with a smaller error tolerance ($< \pm 1^{\circ}\text{C}$) should be selected for future testing.

4.5 Part B - Adiabatic Assumption Investigation

The second goal of the thesis is to investigate an adiabatic expander assumption used in modeling of similar systems. A common assumption within the models used up to this point [50] is that the expander acts as an adiabatic system - that the amount of energy lost to heat transfer from the gas space is negligible. Most ORC systems which are tested today are tested under temperature conditions which are at or near room temperature. However, in automotive applications such a system can be exposed to more severe operating temperatures than in a controlled laboratory experiment. Of interest in automotive applications is the impact that a cold start can have on system performance. The question to be answered is whether the system will be dramatically affected when starting a vehicle at -20°C - and how long it will take the system to reach its optimum performance. A goal of this thesis is to determine whether this assumption is accurate and to quantify the degree to which heat transfer losses affect expander performance.

The measures by which to judge expander performance are mainly the power output and isentropic efficiency of the device. We can expect that colder starting conditions will lower both the power output and isentropic efficiency of the device as the heat transfer losses from the gas to its surroundings will be more severe. Since there is no available experimental data to validate this sort of approach, a purely analytical approach will be employed through the use of the model created. In order to compare the effects of heat transfer on performance, 2 main cases must be run: one adiabatic condition where the effects of heat transfer are ignored, and a second case where heat transfer effects are considered and analyzed. Relevant conditions of each testing case were checked through Engineering Toolbox[49] and a summary of parameters used in all testing conditions in this thesis is provided below in Table 4.2.

| Parameter | All Cases | Parameter | All Cases |
|----------------------------------------|-----------|------------------------------------------|-----------|
| Suction Pressure (bar) | 8.86 | Rotor Mass (kg) | 2 |
| Discharge Pressure (bar) | 1.35 | Casing Mass (kg) | 2.5 |
| Pressure Ratio | 6.5 | Inlet Enclosure Mass (kg) | 0.2 |
| Cylinder Pressure Initial Guess (bar) | 5.5 | Outlet Enclosure Mass (kg) | 0.4 |
| Suction Temperature (K) | 423 | Secondary Component Mass (kg) | 3 |
| Discharge Temperature (K) | 385 | Secondary Envelope Mass (kg) | 3 |
| RPM | 3000 | Rotor Surface Area (m^2) | 0.001 |
| Clearance Volume (cm^3) | 10 | Rotor Thickness (m) | 0.1 |
| Displacement Volume (cm^3) | 55 | Casing Surface Area | 0.0005 |
| Cylinder Temperature Initial Guess (K) | 400 | Casing Thickness (m) | 0.01 |
| Working Fluid | R245fa | h_{conv} Metal - Ambient (W/m^2K) | 200 |
| Cp Gas (J/kgK) | 1100 | Inlet Enclosure Surface Area (m^2) | 0.00012 |
| Cv Gas (J/kgK) | 1038 | Gasket Thickness (m) | 0.01 |
| Gas Constant (J/kgK) | 62 | Secondary Mass Area (m^2) | 0.02 |
| Expander Metal | Aluminum | Envelope Area (m^2) | 0.05 |
| Cp Metal (J/kgK) | 910 | Leakage Area (m^2) | 0.00001 |
| Gas Thermal Conductivity (W/mK) | 0.0125 | Rotor Radius (m) | 0.01 |
| Metal Thermal Conductivity (W/mK) | 220 | Inlet Port Cutoff Angle ($^{\circ}CA$) | 30 |
| Dynamic Viscosity (Pa-s) | 0.00015 | Outlet Port Open Angle ($^{\circ}CA$) | 180 |

Table 4.2: Testing Conditions

For the second and third parts of the analysis, ambient temperature will be taken into account and 3 different temperatures will be simulated. The testing conditions are summarized below in Table 4.3.

| Component | Initial Temperature (K) | | | |
|----------------------|-------------------------|---------------------------------|-------------------------------|--------------------------------|
| | Adiabatic | 250K Ambient ($-23^{\circ}C$) | 275K Ambient ($2^{\circ}C$) | 300K Ambient ($27^{\circ}C$) |
| Rotor | - | 250 | 275 | 300 |
| Casing | - | 250 | 275 | 300 |
| Inlet Enclosure | - | 250 | 275 | 300 |
| Outlet Enclosure | - | 250 | 275 | 300 |
| Secondary Mass | - | 250 | 275 | 300 |
| Envelope Temperature | - | 250 | 275 | 300 |
| Ambient Temperature | - | 250 | 275 | 300 |

Table 4.3: Test Cases

4.5.1 Case 1 - Adiabatic

For this testing case, the effects of heat transfer are ignored. The model calculates the in cylinder conditions and the results converge quickly – usually within 5-10 iterations depending on the initial conditions provided. Results are shown below:

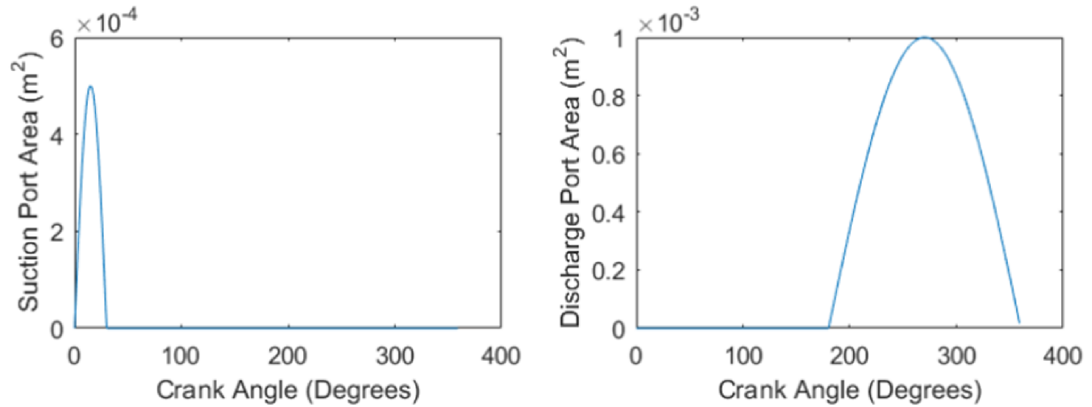


Figure 4.7: Port Surface Areas

The plots of the suction and discharge port areas are shown above in Figure 4.7. They follow a sin function which is an approximation based on supplier data and literature sources such as the work of Brummer[35]. The suction port is open from 0-30°CA to a maximum area of $0.0005m^2$ ($5cm^2$). The discharge port is open from 180-360°CA to a maximum area of $0.001m^2$ ($10cm^2$). Typically, the discharge port of an expander is larger than the inlet port and is open longer to allow the low pressure gas to fully escape from the expansion chamber before the process is complete.

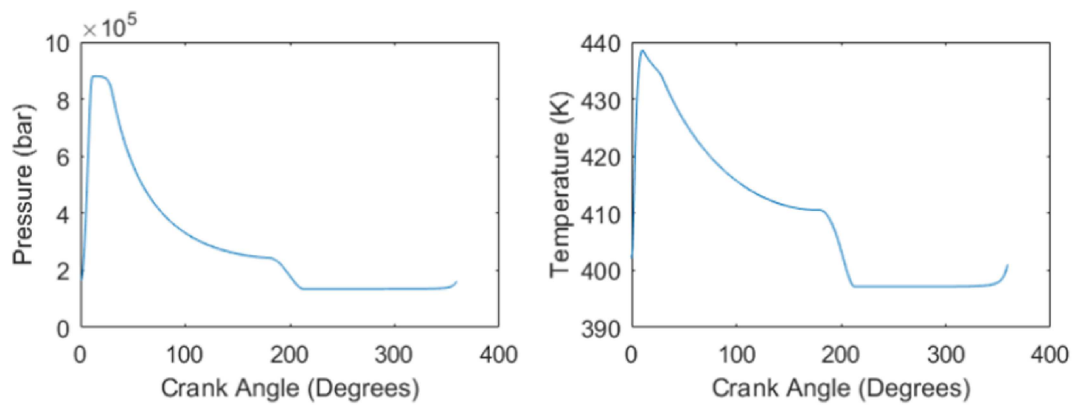


Figure 4.8: Cylinder Temperature and Pressure

The in cylinder pressure and temperature are displayed above in Figure 4.8. They follow a generally similar trend – a sudden increase in pressure and temperature as hot, high pressure gas is allowed into the cylinder while the intake port is open (0-30°CA), followed by a gradual, smooth expansion when both ports are closed (30-180°CA) and the volume in the cylinder increases, followed by a rapid expansion of any gas that has not been expanded once the discharge port is opened (180-360°CA).

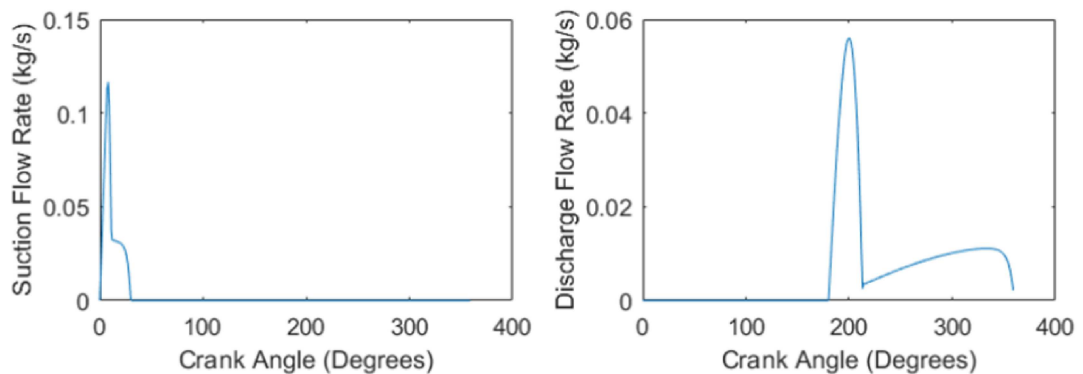


Figure 4.9: Mass Flow Rates

The suction (inlet) and discharge (outlet) flow rates are a result of the opening and closing pattern of the respective ports and are displayed above in Figure 4.9. The suction flow rate has a sharp spike in the beginning of the intake process when the very high pressure gas rapidly enters the port, and begins to fade and level off once

the pressure in the expansion chamber has reached that of the pressure upstream of the expander. The maximum suction mass flow rate is 120 g/s and the average is 43.3 g/s.

Discharge flow rate also has a similar shape, with a sharp spike early in the discharge process due to high pressure gas being exposed to a lower pressure opening. The rapid pressure rise falls once the cylinder pressure reaches the discharge pressure. It begins to increase in a more controlled manner again once the chamber volume decreases and forces the rest of the gas out of the opening. The maximum discharge flow rate is 57 g/s and the average is 11 g/s. The longer duration of the outlet port opening is the reason for the lower peak flow rate and average flow rate.

Note that the suction and discharge mass flow rates are imposed by the difference in pressure between the cylinder gas and the upstream or downstream gas respectively. The equations which govern the mass flow rates are calculated based on the difference in pressure between the cylinder and the inlet or outlet, meaning the mass flow rate is never constant as the cylinder pressure changes. However, in real life testing, the mass flow rate through the system is imposed by the pump and therefore remains relatively constant (a scroll expander is used in this case). The flow rate tested under the conditions above is 30 g/s.

A summary of the results for the adiabatic case is provided below in Table 4.4.

| Parameter | Value |
|-------------------------------|----------|
| Volumetric Efficiency | 87.9% |
| Power | 1.033 kW |
| Isentropic Efficiency | 53.9 % |
| Average Discharge Temperature | 388 K |

Table 4.4: Adiabatic Results

P-V Diagram and Losses

The P-V diagram above provides insight into the amount of work generated throughout the cycle. The area within this curve represents the P-V work done by the gas throughout its expansion process. The P-V diagram also provides a way to visualize the losses encountered in the expander. The P-V diagram for the adiabatic condition is provided below in Figure 4.10.

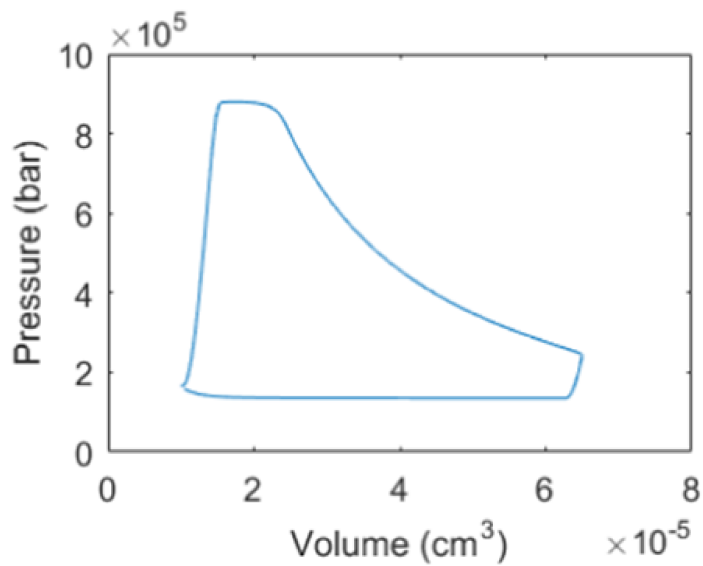


Figure 4.10: P-V Diagram

Leakage, friction and heat transfer (discussed later) are all sources of losses within an expander. As discussed previously, frictional losses in an expander vary depending on expander type and geometry which require specific geometrical details. For the purpose of this thesis, frictional losses are modeled using a mechanical efficiency factor that can be modified by the user. Additionally, heat generated due to friction is accounted for in the heat transfer balance between components.

Below in Figure 4.11 is a P-V diagram of the expander which shows the curve as an idealized model with no losses, and another 2 other curves which consider frictional and leakage losses. All cases were run under the same expander conditions – but

with and without friction and leakage. In the case of leakage, some of the intaken fluid is not expanded and the full potential of the expansion process is not maximized. Friction causes loss through heat generation that is not useful work. Both leakage and friction losses contribute to lower pressures inside the cylinder through the expansion process, leading to less area under the P-V diagram and therefore less work produced.

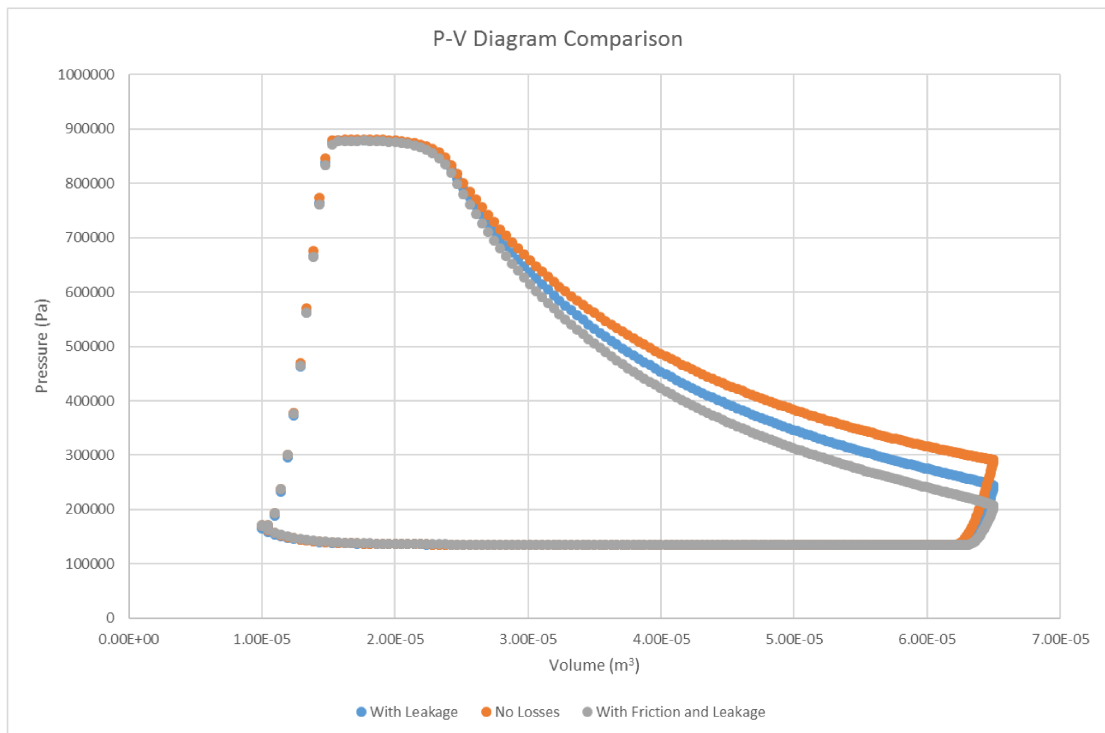


Figure 4.11: P-V Diagram Losses Comparison

Table 4.5 below provides a comparison of the performance losses as a result of friction and leakage. Note that the volumetric efficiency of the device actually increases with leakage since more refrigerant is being taken in as leakage occurs from the cylinder to the discharge port. In some cases, the volumetric efficiency can actually be greater than 1 due to this reason. The isentropic efficiency, power output, and discharge temperature all decrease as a result of the losses incurred through friction and leakage.

| Parameter | No Leakage or Friction | With Friction, No Leakage | With Leakage and Friction |
|-----------------------|------------------------|---------------------------|---------------------------|
| $\eta_{vol}(\%)$ | 85.1 | 83.6 | 87.9 |
| $\eta_{is}(\%)$ | 61.8 | 57.3 | 53.9 |
| $P_{exp}(\text{kW})$ | 1.21 | 1.09 | 1.033 |
| $T_{d,avg}(\text{K})$ | 395.3 | 393.8 | 387.9 |

Table 4.5: Losses Comparison

4.5.2 Case 2 - With Heat Transfer

The purpose of this section is to determine whether heat losses in the expander are substantial and whether the adiabatic expander assumption is correct. For this reason, the results of the 300K ambient temperature case are chosen as they demonstrate the minimum amount of heat transfer loss of the cases examined. As the simulation iterates, the temperatures of the expander components will heat up due to gas expansion. In order to examine the full effect of heat transfer, the simulation is only run until convergence is first reached – between 3-5 iterations. This allows us to capture the worst case scenario of heat transfer loss when the components are at their coldest (initial ambient conditions).

Results at 300K (27C)

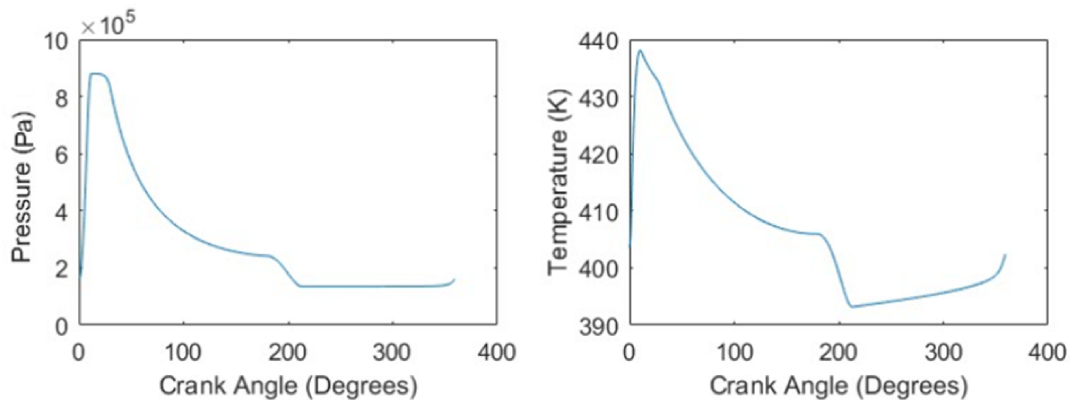


Figure 4.12: In Cylinder Temperature and Pressure 300K

Figure 4.12 above depicts the in-cylinder temperature and pressure of the final iteration of the simulation. The other parameters (mass flow rate, suction and discharge areas) are the same as the adiabatic case. Notice the level of similarity of the results to the adiabatic case once convergence has been reached. While we expect the results to be slightly different with the effects of heat transfer considered, the general shape of the plots should be quite similar. This is due to the definition of steady state conditions – once all the components have reached their steady state temperature, there will still be heat loss to the ambient environment but not to the mechanical components of the device. For this reason, we anticipate that the results at steady state should be similar. A lower minimum temperature can be observed in the temperature plot due to lower ambient conditions tested at this case.

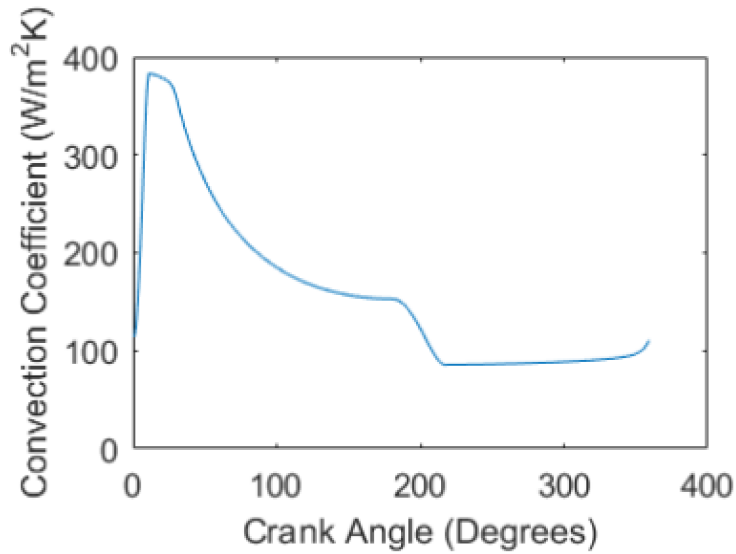


Figure 4.13: Convection Coefficient

Figure 4.13 above depicts the evolution of the convection coefficient over the crank cycle. We see that the heat transfer coefficient follows a trend almost identical to that of the pressure trace in the cylinder. This is due to the dependence of the convection coefficient on the density of the fluid in the cylinder as described in Section 3.3.4. Since the density is tied to the cylinder pressure through the ideal gas law, the heat

transfer coefficient plot looks very similar to the pressure trace.

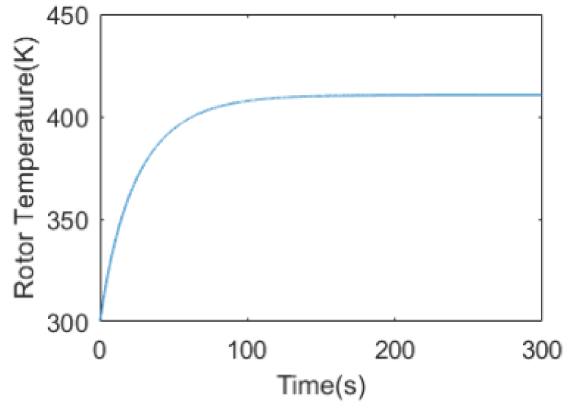


Figure 4.14: Rotor Temperature 300K Case

Figure 4.14 above displays the temperature of the rotor with time. We can see that the rotor temperature increases gradually from its initial temperature of 300K to its maximum temperature of 405 K once heat transfer to the rotor reaches 0.

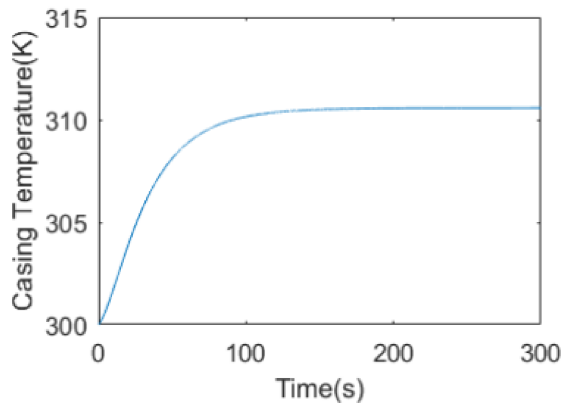


Figure 4.15: Casing Temperature 300K Case

Figure 4.15 displays heat transfer to the casing. The casing temperature increases from its original temperature of 300K to its maximum of 311K as the heat transfer to the rotor decreases to 0. The casing temperature is much cooler than the rotor temperature shown above due to the cooling effect that the ambient air has on the casing metal. While the rotor is only exchanging heat with the working gas space,

the casing is exposed to ambient air through convection on its outer wall. This has a cooling effect on the casing and results in lower peak temperature.

The rest of the components follow comparable trends as they interact with each other during the heating process. Their respective plots are shown below in Figure 4.16. Their temperatures increase at different rates depending on the nature of their interactions with the other components through conduction or convection.

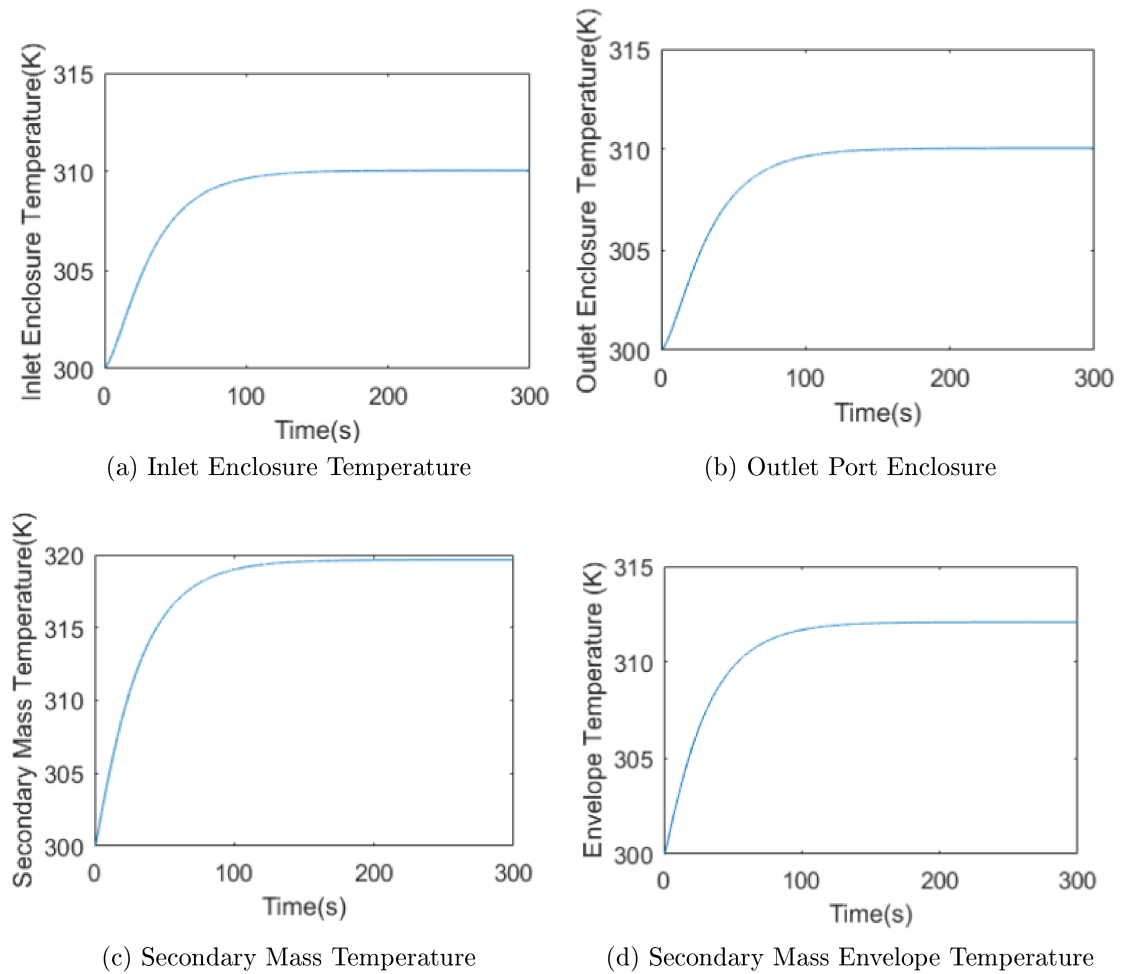


Figure 4.16: Components Temperatures 300K

Table 4.6 below summarizes the differences in performance between the adiabatic case and the case involving heat transfer.

| Parameter | Adiabatic | Heat Transfer |
|-----------------------------------|-----------|---------------|
| Volumetric Efficiency (%) | 83.6 | 88.3 |
| Isentropic Efficiency (%) | 53.9 | 51.0 |
| Power (kW) | 1.033 | 0.977 |
| Average Discharge Temperature (K) | 387.9 | 392.9 |

Table 4.6: Heat Transfer Performance Comparison

The analysis shows that heat transfer losses can account for a 3% drop in isentropic efficiency within the expander which corresponds to a drop of roughly 70W of output power. While these losses are fairly small, they should be considered if the goal of the simulation is a very accurate performance evaluation. However, automotive manufacturers are mainly concerned with overall vehicle fuel economy improvements. A 3% decrease in isentropic efficiency will have no meaningful effect on vehicle fuel economy, so any reduced simulation time through use of a simplified, adiabatic model is justified.

Note that this comparison is between an adiabatic case and fully cold expander condition. The performance was recorded after only a few revolutions of the machine to capture the lowest point in expander performance. The reason is to capture the amount of heat loss encountered at the maximum loss point when the machine is at its coldest. As the machine heats up, its performance will improve until it reaches a steady state temperature condition with the environment. The following section will look at how much the machine performance improves while warming up.

4.6 Part C - Rotor and Casing Temperature vs. Performance

By examining the performance of the expander as a function of the temperatures of its components, it is possible to quantify the effect of a cold start on the machine. The plots below show the performance of the expander as a function of the temperatures of the two components it is in contact with: the rotor and the casing.

3 different cases were run: ambient temperature at 300K (27°C), 275K (2°C), and

250K(-23°C). The results from each case will be presented and compared below. For this section, only the performance plots as a function of component temperature are shown – in cylinder temperature and pressure diagrams show no substantial difference to the plots already shown at steady state.

4.6.1 Case 1 - 300 K Ambient Temperature

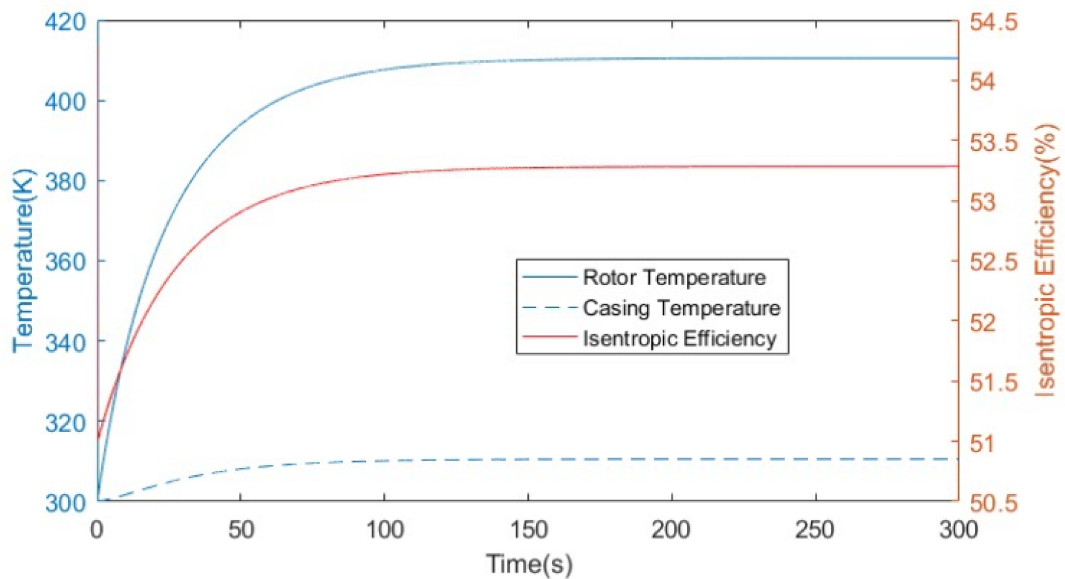


Figure 4.17: Isentropic Efficiency 300K

Figure 4.17 displays the isentropic efficiency at 300K. As the temperature of the rotor and casing increases, the efficiency of the expander increases due to diminishing heat transfer losses to the environment. A lower temperature difference between expander and the ambient lowers heat transfer and therefore improves expander performance.

While we can see that there is a correlation between the rotor and casing temperatures and the isentropic efficiency of the device, the correlation is relatively weak. Under a completely cold start, the expander efficiency is at 51.0%. At fully warm conditions and maximum performance, the expander achieves an isentropic efficiency of 53.3%. Another note here is that the 53.3% isentropic efficiency is a 0.6% drop

compared to the adiabatic case analyzed above. 0.6% drop corresponds to the constant amount of heat loss that is lost at steady state conditions when all components have reached their full operating temperature.

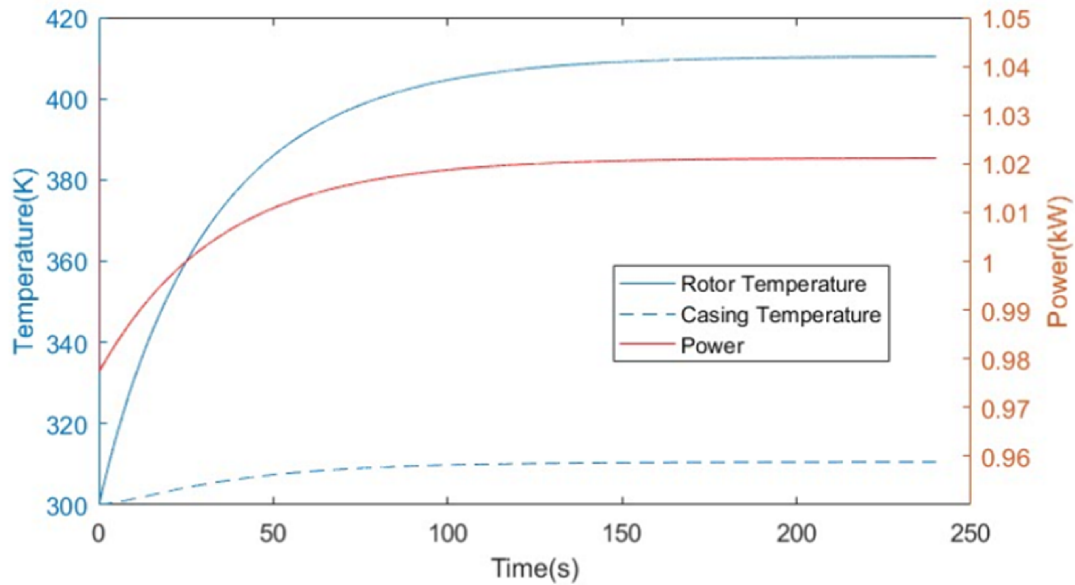
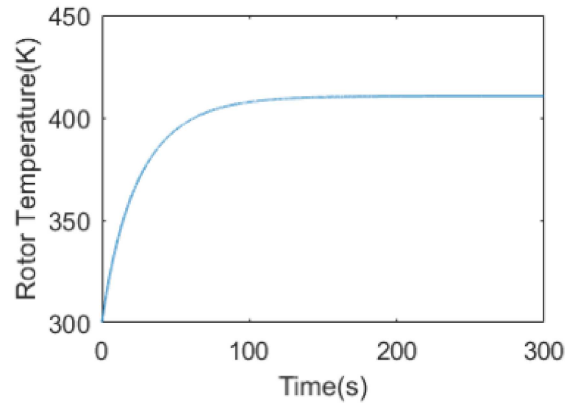


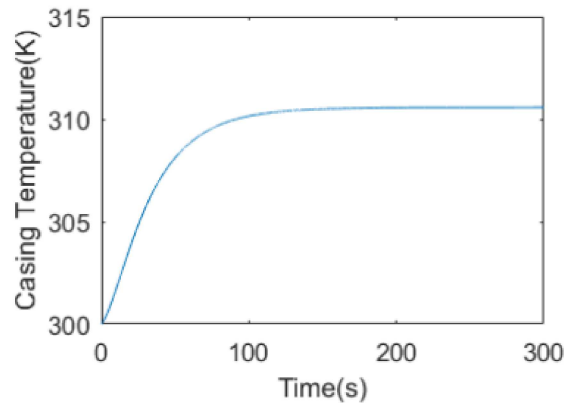
Figure 4.18: Power 300K

From the plot of expander power vs. casing and rotor temperature shown above in Figure 4.18, a power increase of approximately 40 W (1021W-980W) can be seen from cold to fully warm conditions. While not a negligible amount, the overall contribution is relatively small.

The temperatures for the rotor and casing in the 300K ambient temperature case are shown below in Figure 4.19:



(a) Rotor Temperatures 300K



(b) Casing Temperature 300K

Figure 4.19: Rotor and Casing Temperatures 300K

The rotor is the component with the greatest effect on expander performance as it has direct contact with the working space, and no cooling presence such as ambient air. The rotor temperature increases from 300K initially to 405K at steady state conditions. The casing temperature follows a similar trend but reaches a much lower steady state temperature due to the cooling effect of ambient air on the outside of the metal.

The temperatures for the rest of the components are shown in the appendices. They follow similar trends to plots already seen as they interact with each other and transfer heat across their lumped masses. Their effect on expander performance is dramatically less than that of the casing and rotor and can be considered virtually

negligible.

4.6.2 Case 2 - 275 Ambient Temperature

The results below depict an ambient temperature of 275K.

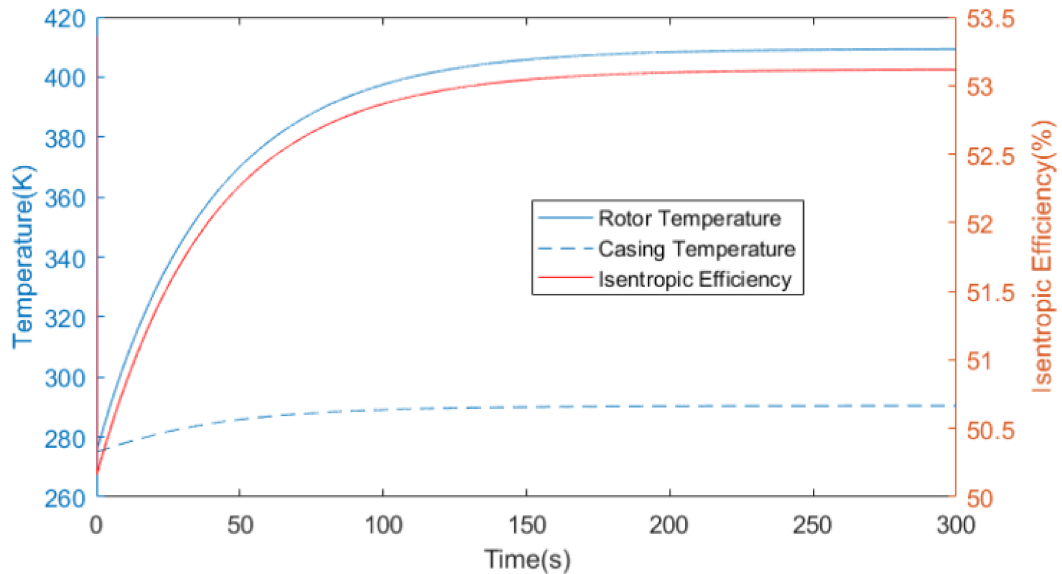


Figure 4.20: Isentropic Efficiency 275K

The isentropic efficiency as a function of rotor and casing temperature can be seen above in Figure 4.20 for the 275K ambient temperature case. We can see that the isentropic efficiency begins at a slightly lower value than the 300K case due to the difference in temperature which causes higher heat losses while the machine is heating up. However, nearly the same isentropic efficiency is reached at steady state. The reason for the difference in isentropic efficiency (and power) is the increased steady state heat loss due to colder ambient conditions. At steady state, the expander will lose more heat under ambient conditions at 275K than at 300K due to a larger temperature difference.

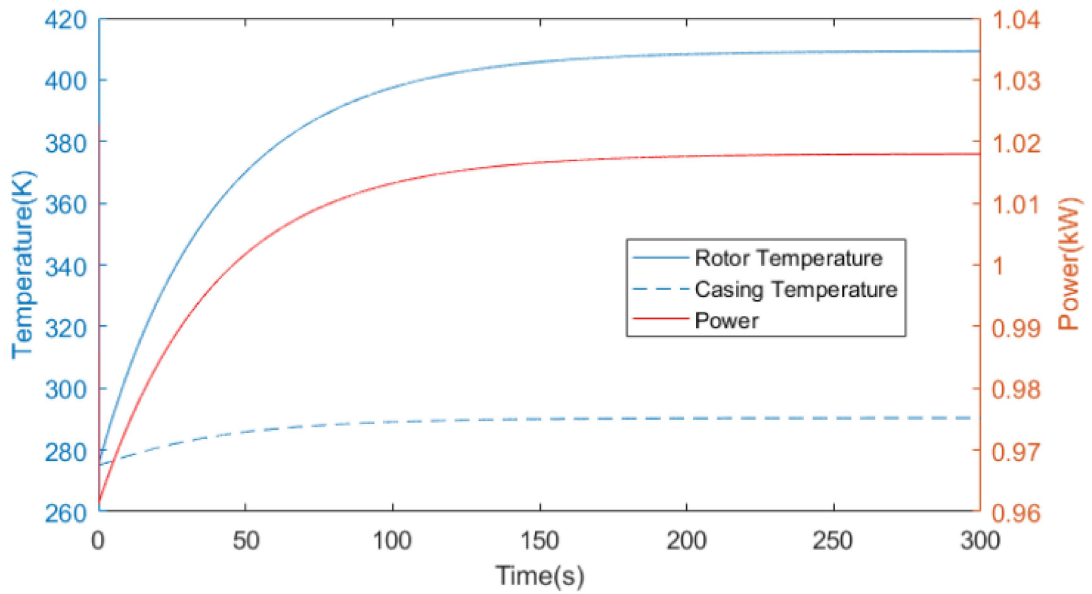
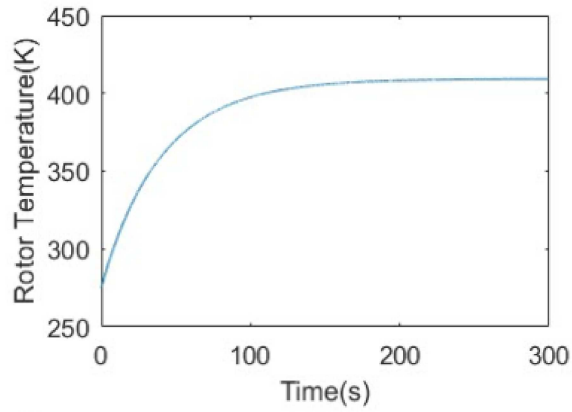


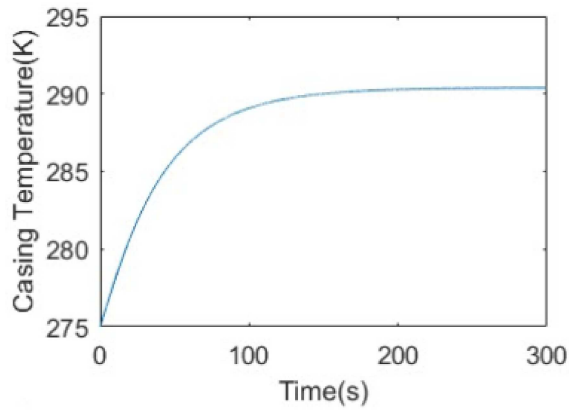
Figure 4.21: Power 275K

Similarly, the power will follow a similar trend to isentropic efficiency as shown in Figure 4.21. Compared to the 300K ambient temperature case, the power output starts and ends slightly lower in the 275K case than the power output at the 300K case due to increased heat transfer losses with the environment at steady state.

The plots of temperature of each of the components will be similar to the first case. Below in Figure 4.22 are the temperatures of the rotor and casing for the 275K case.



(a) Rotor Temperatures 275K



(b) Casing Temperature 275K

Figure 4.22: Rotor and Casing Temperatures 275K

The temperatures of the rest of the components are shown in the appendices. They follow similar trends to plots already seen as they interact with each other. Their effect on expander performance is dramatically less than that of the casing and rotor.

4.6.3 Case 3 - 250K Ambient Temperature

The results below depict an ambient temperature of 250K.

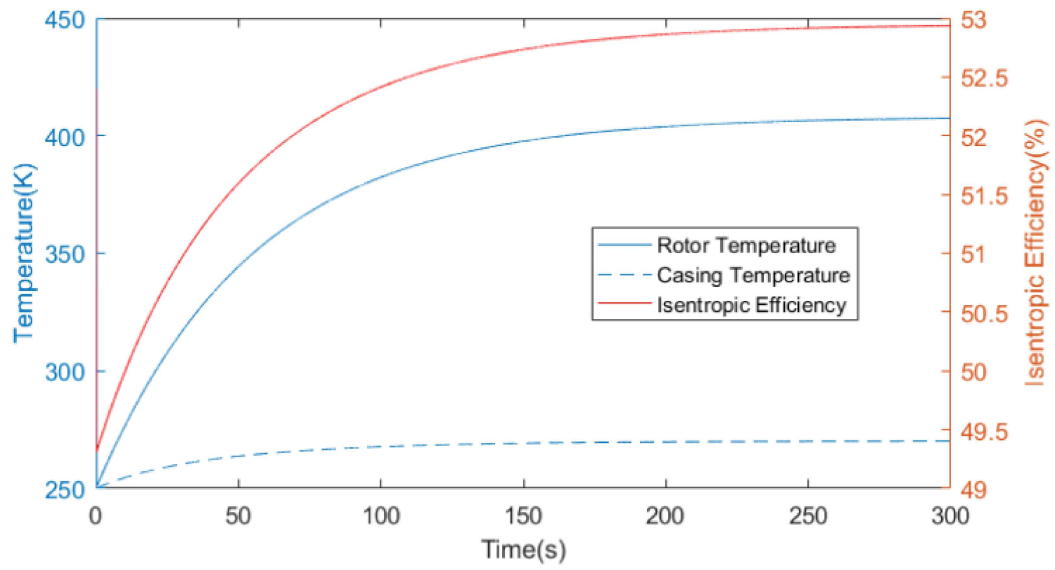


Figure 4.23: Isentropic Efficiency 250K

For the third case with an ambient temperature of 250K, we are examining an extreme weather case. The isentropic efficiency plot is shown above in Figure 4.23. A situation like this could be found while starting a vehicle on a cold day in winter. The isentropic efficiency at completely cold conditions is 49.3%, and 52.9% at steady state.

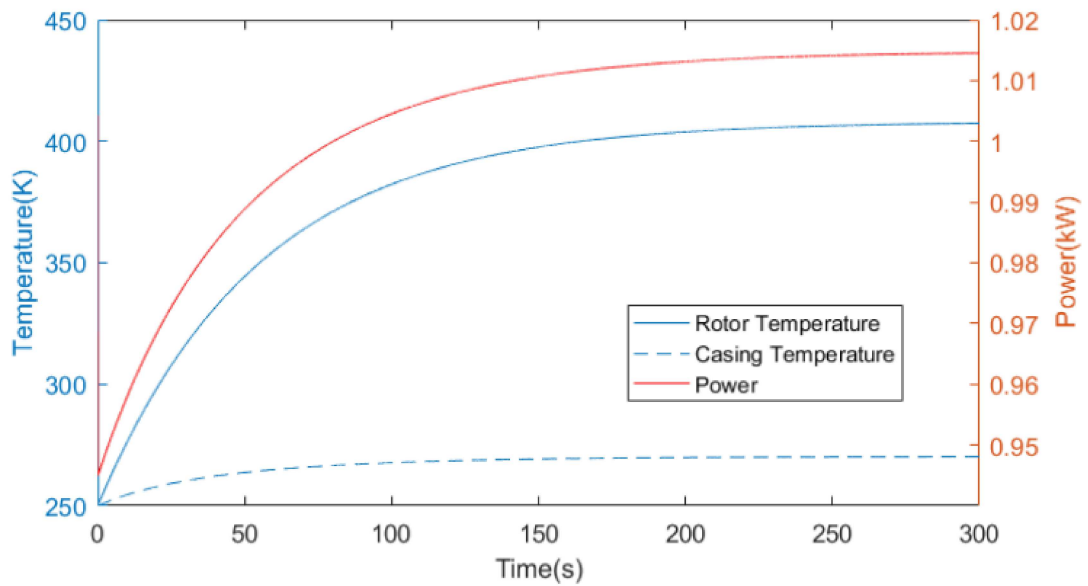
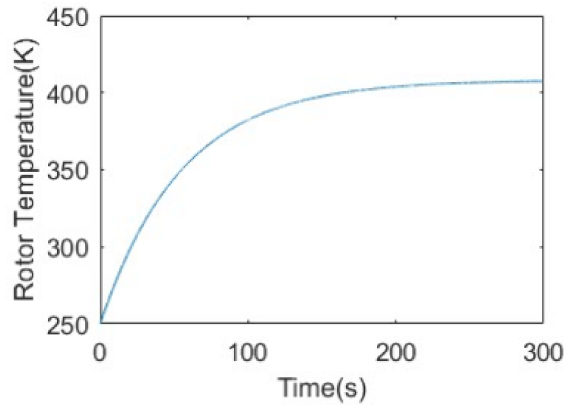


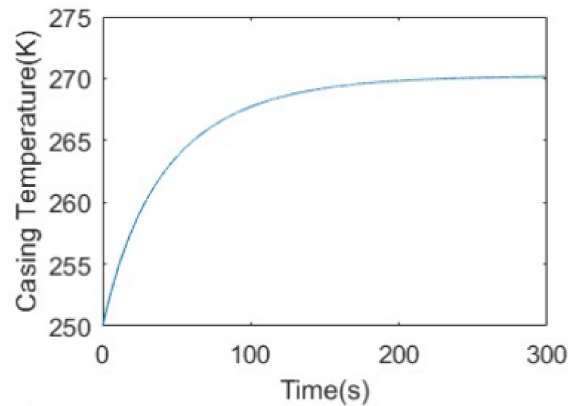
Figure 4.24: Power 250K

Figure 4.24 above shows the power as a function of temperature. The power output begins at 0.944 kW at cold conditions and reaches 1.015 kW at steady state conditions.

Similarly, the plots of temperature of each of the components will be similar to the first case. Below in Figure 4.25 are the temperatures of the rotor and casing for the 250K case.



(a) Rotor Temperatures 250K



(b) Casing Temperature 250K

Figure 4.25: Rotor and Casing Temperatures 250K

The temperatures of the rest of the components are shown in the appendices. They follow similar trends to plots already seen as they interact with each other. Their effect on expander performance is dramatically less than that of the casing and rotor and are virtually negligible.

4.6.4 Comparison of Performance

Figure below depicts a comparison of the 3 cases simulated.

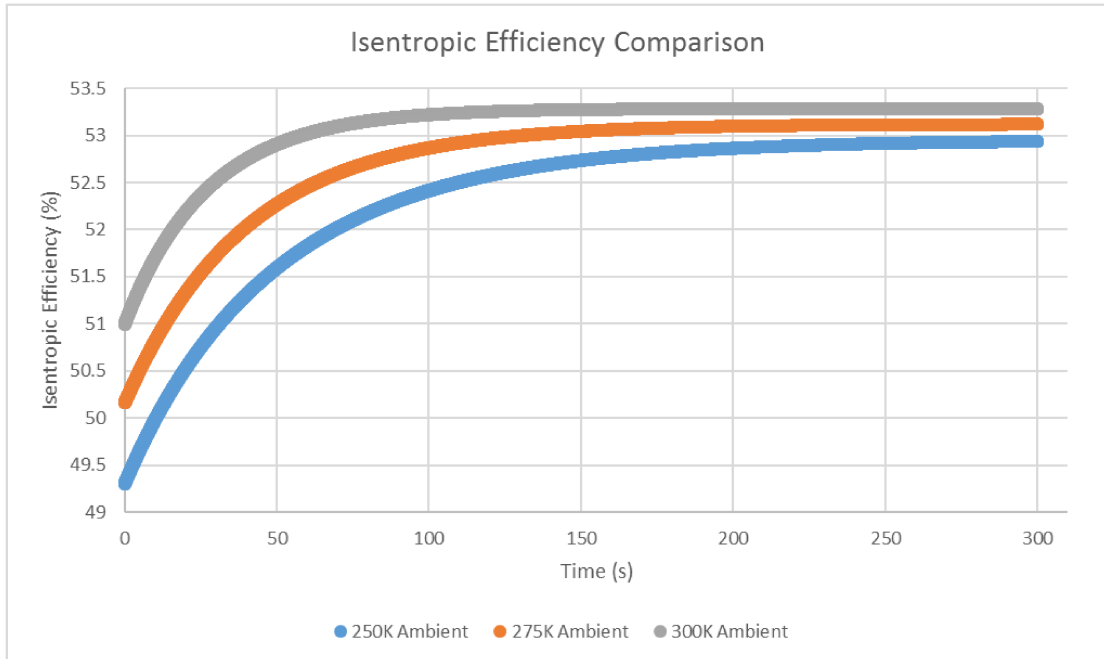


Figure 4.26: Isentropic Efficiency Comparison

Figure 4.26 above provides a comparison of isentropic efficiency over the 3 test conditions. By comparing the isentropic efficiency of the expander under the 3 simulated cases, we can see that a higher ambient temperature results in a higher expander efficiency. This is due to lower heat losses as a result of a smaller temperature difference between the expander and its ambient environment. A larger initial temperature difference causes the differences in efficiency at the start of the simulation, but the gap between cases becomes smaller as the components heat up after operating for some time. Once they have reached steady state conditions, the difference in efficiency is due to more steady state heat loss to the environment under colder conditions. We can see that at steady state, the machine is operating at nearly the same performance regardless of ambient temperature – the difference in efficiency at steady state is less than 0.5% between the 250K case and 300K case.

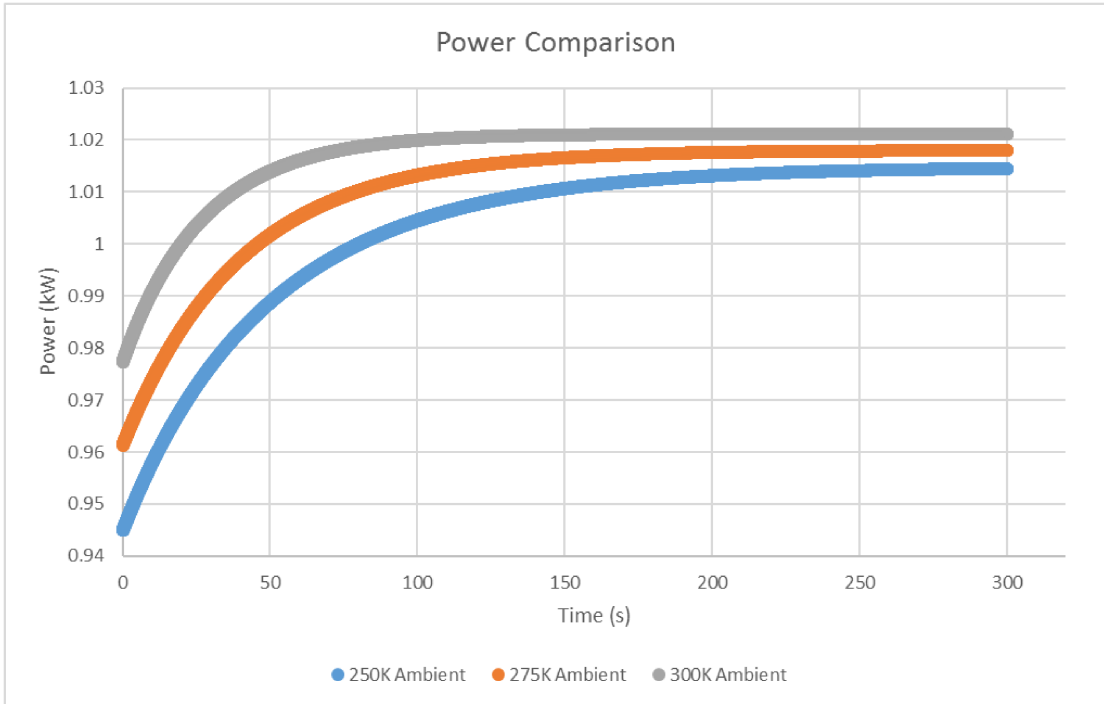


Figure 4.27: Power Comparison

The expander power output naturally follows a similar trend as the isentropic efficiency as they are intrinsically linked as shown in Figure 4.27 above. At startup, the difference in power output is due to greater heat loss to the environment due to a greater temperature difference between expander and the ambient. The difference diminishes as the expander temperature increases. At steady state, the difference in power between the 300K and 250K ambient temperature case is less than 10W due to increased steady state heat loss at lower ambient temperatures.

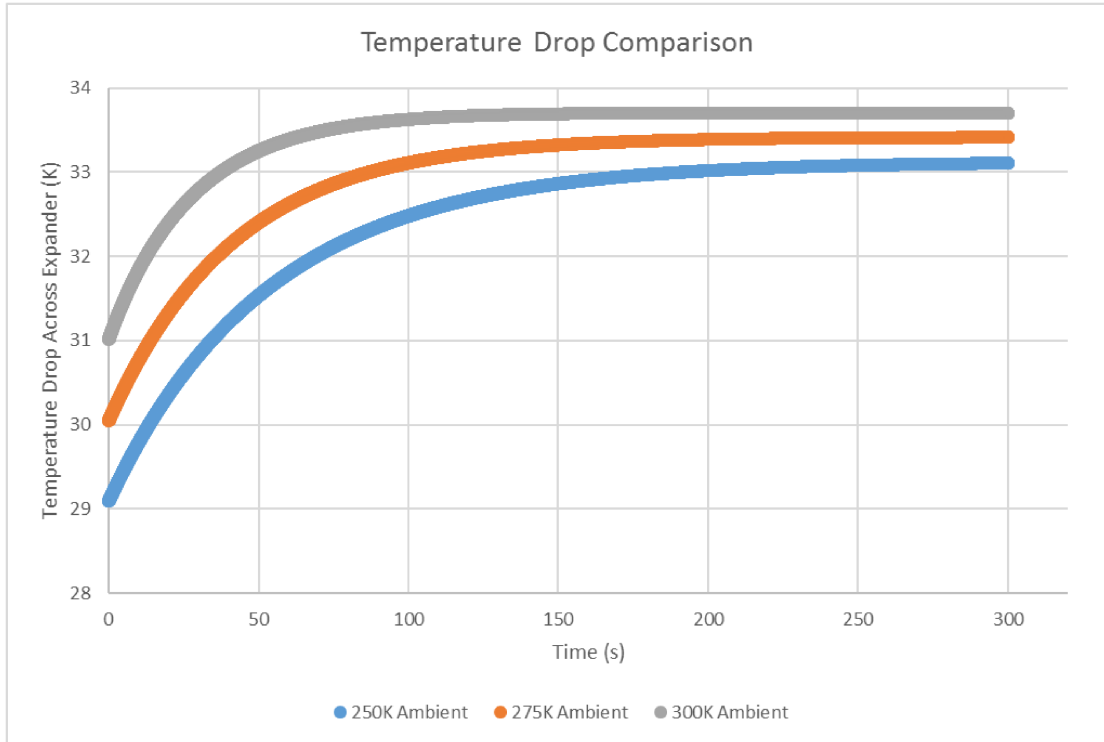


Figure 4.28: Temperature Drop Across Expander Comparison

The comparison of the temperature drop over the expander is shown in Figure 4.28. Similar to the isentropic efficiency and power curves, the temperature drop across the expander increases with increasing ambient temperature. For a constant inlet temperature, a greater temperature difference across the expander would be indicative of more power being produced. Therefore, the temperature drop over the expander is another indicator of expander performance and another way to check whether the trend is captured correctly. The plot resembles the same trend seen in both the isentropic efficiency and power plots above.

4.6.5 Summary

Table 4.7 below provides a summary of the evolution of the performance of the expander under the 3 different simulated cases.

| Parameter | 300K Ambient | | 275K Ambient | | 250K Ambient | |
|---------------------------|--------------|-------|--------------|-------|--------------|-------|
| | Start | End | Start | End | Start | End |
| Isentropic Efficiency (%) | 51 | 53.3 | 50.16 | 53.11 | 49.3 | 52.95 |
| Power (kW) | 0.977 | 1.012 | 0.961 | 1.018 | 0.944 | 1.015 |
| Temperature Drop (K) | 31 | 33.7 | 30.1 | 33.4 | 29.1 | 33.1 |

Table 4.7: Comparison Summary

4.6.6 Time to Full Performance

Contrary to most ORC applications which have been analyzed today, automotive applications can involve scenarios where a vehicle must be started under cold operating conditions. In an extreme example, of interest is how the system operates and to what degree a -20°C ambient temperature affects expander performance. Knowing how the temperature of expander components affects the performance of the system can assist in making decisions specific to automotive applications. A critical parameter is the time it takes the system to reach its optimum level of performance to know when to potentially engage the system to avoid being wasteful.

The model has the ability to predict such a time. For example, we can compare the times needed to full performance under 3 different starting temperatures – if the ambient temperature is roughly -20°C , 0°C , and 20°C . This can provide an estimate of when to potentially engage the system under various temperatures to ensure maximum performance. Once the heat transfer to each respective component is 0, steady state has been reached and the time needed for this to happen can be analyzed. Additionally, the time constant for the expander under different temperatures can be analyzed. The time constant is defined as the time required for an object to reach 63.2% of its final value[56]. In this case, the time constant is represented by the time the expander requires to reach 63.2% of its steady state temperature while warming up. This analysis is useful in the design of control systems for ORC testing.

We will consider full performance once the power output has been maximized

for each case. The highest isentropic efficiency, power output, and lowest discharge temperature will all coincide at the same time. The rotor is usually the component which takes the longest to reach steady state because of the absence of a cooling presence from the ambient environment. By observing when the temperature of the rotor reaches its maximum, we can see when steady state conditions have been met and therefore when maximum expander performance will be achieved.

Figure 4.29 below provides a plot of the rotor temperature vs. time for the three simulated cases. As the component which has the highest effect on expander performance due to its high temperature and proximity to the working gas space, the rotor is the most critical component to analyze for steady state conditions. We expect that the time required to reach full performance should increase as the ambient temperature decreases. It should take longer for a component starting at 250K to reach its full operating temperature than a component at 300K. It is clear that colder ambient conditions result in a longer heating up process of the rotor. The rotor under the 300K ambient case has reached steady state temperature while the others are still warming up. Each of the 3 cases will be compared individually below.

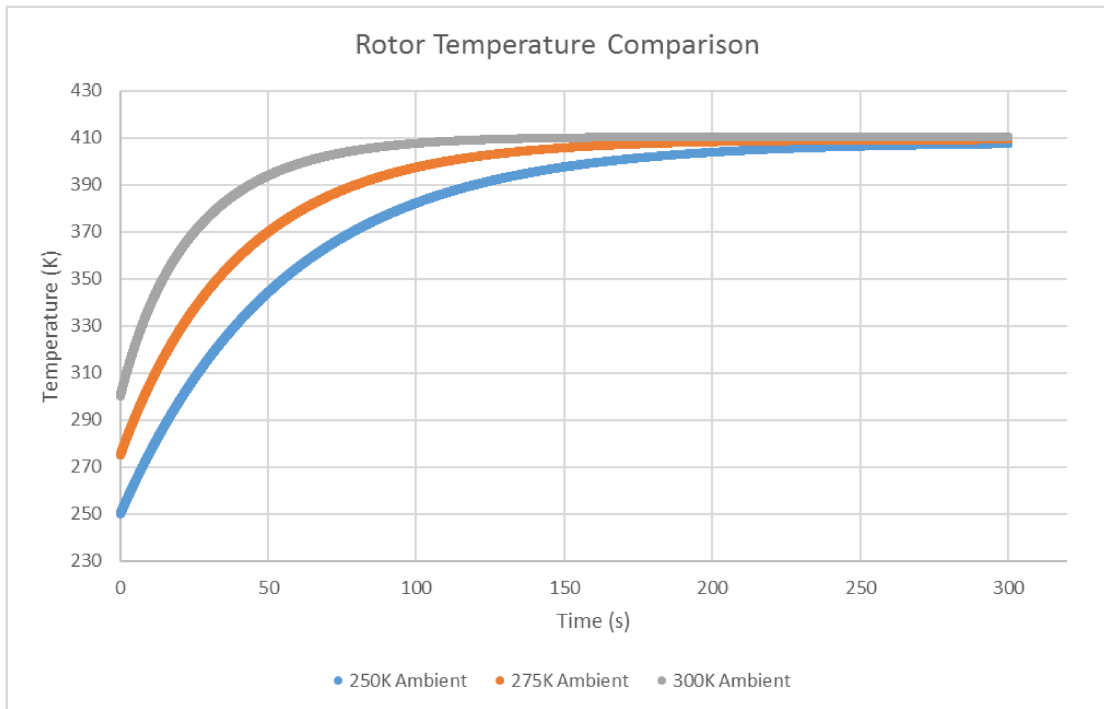


Figure 4.29: Rotor Temperature Comparison

The rotor temperatures for each of the 3 cases are depicted below. The red marker on each plot shows the time at which the rotor temperature has reached steady state as heat transfer to the environment trends to zero. The green marker represents the time at which the temperature of the rotor is at 63.2% of its final value for evaluating the time constant. As expected, the amount of time needed to reach steady state increases with decreasing temperature. This is logical as it is expected that a system at an ambient temperature of 250K would require a longer time to reach steady state than a system starting at 300K.

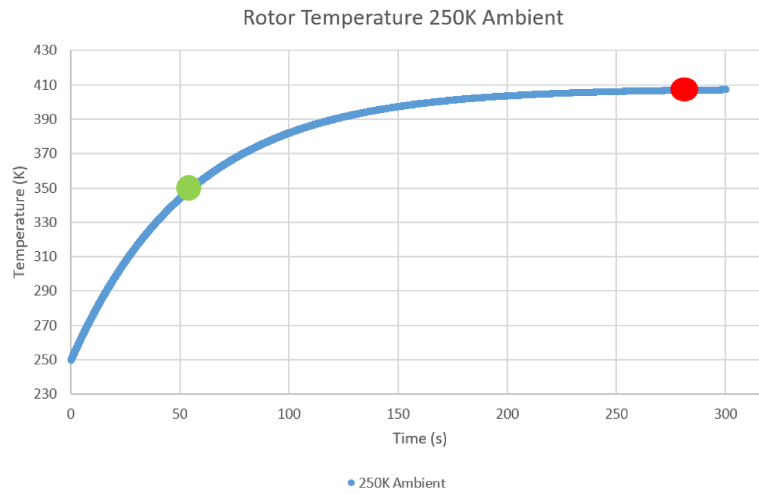


Figure 4.30: 250K Rotor Temperature

Figure 4.30 above displays the 250K ambient temperature case. The time needed to reach full performance is 280 seconds, and the time constant is 52 seconds.

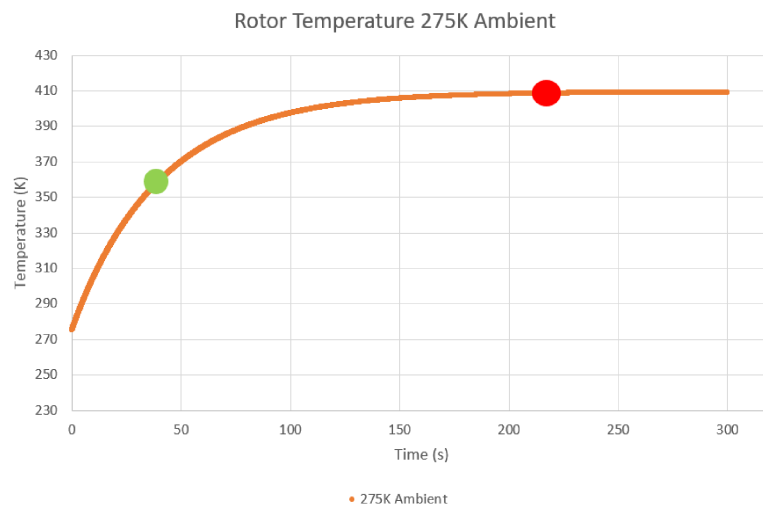


Figure 4.31: 275K Rotor Temperature

Figure 4.31 above displays the 275K ambient temperature case. The time needed to reach full performance is 220 seconds, and the time constant is 43 seconds.

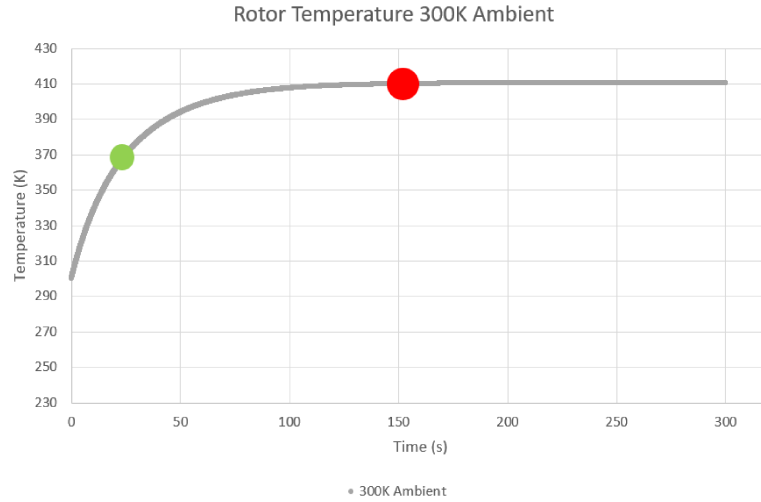


Figure 4.32: 300K Rotor Temperature

Figure 4.32 displays the 300K ambient temperature case. The time needed to reach full performance is 150 seconds, and the time constant is 27 seconds.

This analysis provides a method for calculating the time needed for the expander to reach its optimal performance level. This is especially important under cold start conditions where ambient temperature can cause substantial performance problems. We can conclude from these plots that in order to receive the greatest possible benefit from the expander, the system should be engaged after approximately 2.5 minutes at 300K, 3.5 minutes at 275K, and 4.5 minutes at 250K. Table 4.8 below summarizes the results of the 3 test cases.

| Ambient Temperature | τ (s) | t_{FP} (s) |
|---------------------|------------|--------------|
| 250K | 52 | 280 |
| 275K | 43 | 220 |
| 300K | 27 | 150 |

Table 4.8: Summary of Warm-up Times

The time constant is not uniform along the 3 cases - it is used to determine the thermal time scale of the expander as needed for system level model assumptions. Since the time constant is considerably greater than a few seconds, it can be concluded

that the expander heats up dramatically slower than the heat exchangers within the ORC, and that its thermal transients can be ignored for dynamic control purposes.

5 Conclusion and Recommendations

5.1 Summary

The Organic Rankine Cycle is a promising waste heat recovery technology with the potential for substantial fuel savings when used in automotive applications. As the power producing device within the system, the expander plays a critical part in maximizing overall cycle efficiency. The aim of this thesis is the development of a generic, modular expander model which acts as a thermodynamic template for expander performance. Generic geometric relationships are chosen for calculations within the model which are representative of general expander operation. The user is given the ability to modify key model parameters such as volume and port surface area relationships through user defined Matlab functions which allow for differentiation between various expander types and geometries. A heat transfer analysis is performed at each mechanical component within the expander to evaluate the effect that each part has on the working gas space properties.

Goals of the simulation are:

1. Provide the ability to examine the performance of different expander types and geometries
 - A generic, modular approach is chosen to give the user the ability to differentiate between expander types through customizable functions. User inputs such as chamber volume, port surface area, lumped mass surface area and masses are user-defined and fulfill the goal of creating a tool which can be used for the analysis of various geometries.
2. Examine expander heat transfer through an analysis of the thermal behaviour of its mechanical components
 - A heat transfer balance is performed at each mechanical component to

examine its respective effect on the thermal behaviour of the device. This goal is achieved by providing a time history of each component temperature over its operating range and observing their respective effects on expander performance.

3. Create a detailed physics-based model to be used as a benchmark for simpler models
 - The generic simulation tool is used as a detailed tool to calibrate simpler models which are not examined in this thesis. The detailed model outlined in the thesis acts as a benchmark for simpler, less time consuming models implemented in industry due to the need for low computational times.

Within the framework of the 3 main goals of the thesis, there are 3 main applications which are examined in detail in the results section of this document which demonstrate how the model is used to solve the outlined thesis goals. All goals outlined at the beginning of the thesis work have been met successfully.

- Part A - To evaluate the sensitivity of expander shaft output power on downstream temperature readings. Calculations from testing results show that the output power and isentropic efficiency of the expander have a large sensitivity to downstream temperature readings, which can lead to unreasonable values of power and isentropic efficiency. The model can be used as a tool to evaluate the amount of error produced by changes in discharge gas temperature in order to assist in experimental design decisions.
- Part B - To evaluate the validity of the adiabatic expander assumption. Models found in literature often assume the expander is adiabatic - that heat transfer losses are negligible. Heat transfer analysis in the model can determine whether this assumption is valid.

- Part C - To evaluate the degree to which temperature affects expander performance. By evaluating the performance of the expander as a function of the temperature of its components, the degree to which ambient temperature affects expander performance can be quantified.

5.2 Results and Recommendations

From Part A – error analysis, it can be seen that the model is a tool which can contribute to the experimental testing procedure. Results provide an average error of 5% per degree change in discharge gas temperature. With an error tolerance of $\pm 2.2^{\circ}\text{C}$ for the current thermocouple that was selected, errors in shaft power can reach in excess of 20%. The recommendation is to obtain a higher quality thermocouple with a smaller error tolerance in order to improve the quality of the results obtained. An ideal thermocouple would limit temperature reading error to within $\pm 1^{\circ}\text{C}$.

From Part B – adiabatic assumption, the model shows the significance of heat transfer on expander performance. Losses in isentropic efficiency of up to 3% can be seen through simulation, meaning that heat transfer losses should be considered in a very detailed model - but can be considered mostly negligible for automotive applications where overall vehicle fuel economy is important. The recommendation is that the adiabatic assumption should be considered in future detailed modeling attempts. However, in applications where minimizing computational time is important, the adiabatic expander assumption is justified.

From Part C – time to full performance, we can view the isentropic efficiency and power output of the device as a function of the temperature of its components. By analyzing the amount of time the system requires to reach optimum performance, recommendations regarding when to engage such a system under potentially cold start conditions can be made. In the three cases analyzed (300K, 275K, and 250K ambient temperature) the amount of time required for the system to reach optimum

performance is 150 seconds, 220 seconds, and 280 seconds respectively. To achieve maximum benefit, the system should be engaged after the respective amount of time has passed for each case. The calculation of time constants for the 3 simulated cases shows that the warm-up time of the expander is considerably greater than that of ORC system level heat exchangers (a few seconds). Therefore, the thermal transients of the expander can be ignored for dynamic system level control schemes. Additionally, research into expander materials which improve the thermal transient performance of the device could provide significant performance benefits for future systems.

Appendices

List of NIST equations used for calculation of spreadsheet parameters:

1. Saturation temperature for R245fa

$$T_{sat} = \frac{2435.8}{9.903 - \log P} - 42.2$$

2. Superheated vapour enthalpy for R245fa

$$h_{vap} = h_{sat} + a(SH) + b(SH)^2$$

$$h_{sat} = h_{liq}(T_{sat}) + h_{fg}(T_{sat})$$

$$a = 0.785144 + 0.0984818P - 0.0128824P^2 + 0.00112715P^3 - 0.0000481627P^4 + 0.000000788906P^5$$

$$b = 0.00297331 + 0.016129x + 0.0236278x^2 - 0.182341x^3 + 0.202346x^4$$

$$x = 1 - \left(\frac{T_{sat}}{427.2} \right)$$

3. Amount of superheat

$$SH_{vap} = \frac{-a + \sqrt{a^2 + 4b(h - h_g)}}{2b}$$

4. Entropy

$$S_{vap} = c + dh_{vap} + eh_{vap}^2$$

$$c = 0.0898213 - 3.827x - 27.693x^2 - 144.1x^3 + 466.8x^4 - 805.9x^5 + 570x^6$$

$$d = 0.0030235 + 0.0164237x - 0.067134x^2 + 0.1753x^3 - 0.164844x^4$$

$$e = -0.00000101254 - 0.0000199116x + 0.0000869053x^2 - 0.000238892x^3 + 0.000228088x^4$$

$$x = 1 - \left(\frac{T_{sat}}{427.2} \right)$$

5. Isentropic enthalpy change

$$h_{isen} = f \cdot \log \left(\frac{P_{in}}{P_{out}} \right)$$

$$f = -8.9497 + 26.598 \cdot S_{vap}$$

References

- [1] Orr, B. "A Review of Car Waste Heat Recovery Systems Utilising Thermoelectric Generators and Heat Pipes." *Applied Thermal Engineering* 101 (2015): 490-95.
- [2] Sung-Wei, Hsu. "Experimental Investigation of the Performance of a Hermetic Screw-Expander Organic Rankine Cycle." *Energies* 7 (2014): 6172-185.
- [3] Dickes, Rémi; Dumont, Olivier; Declaye, Sébastien; Quoilin, Sylvain; Bell, Ian; and Lemort, Vincent, "Experimental Investigation Of An ORC System For A Micro-Solar Power Plant" (2014). International Compressor Engineering Conference. Paper 2372.
- [4] Brasz, Joost J. "Power Production from a Moderate -Temperature Geothermal Resource." GRC Annual Meeting (2008).
- [5] Dickes, Remi. "Design and Fabrication of a Variable Wall Thickness Two-stage Scroll Expander to Be Integrated in a Micro-solar Power Plant." Master's Thesis (2013).
- [6] Lemort, Vincent. "Contribution To The Characterization Of Scroll Machines In Compressor And Expander Modes." PhD Dissertation (2008).
- [7] Sylvain Quoilin, Sébastien Declaye, Bertrand F. Tchanche, Vincent Lemort. Thermo-Economic optimization of waste heat recovery Organic Rankine Cycles. *Applied Thermal Engineering*, Elsevier, 2011, 31 (14-15), pp.2885.
- [8] "ORC Technology." Exergy ORC. <http://exergy-orc.com/technology/orc>

- [9] Kapooria, RK. "An Analysis of a Thermal Power Plant Working on a Rankine Cycle: A Theoretical Investigation." *Journal of Energy in Southern Africa* 19 (2008).
- [10] Brasz, Lars J. and Bilbow, William M., "Ranking of Working Fluids for Organic Rankine Cycle Applications" (2004). *International Refrigeration and Air Conditioning Conference*. Paper 722.
- [11] Capano, Gianmarco. "Waste Heat Recovery Systems for Fuel Economy." *Master's Thesis* (2013).
- [12] Kaplan, Uri. "Organic Rankine Cycle Configurations." *Proceedings European Geothermal Congress 2007* (2007).
- [13] Quoilin, Sylvain. "Techno-economic Survey of Organic Rankine Cycle (ORC) Systems." *Renewable and Sustainable Energy Reviews* 22 (2013): 168-86.
- [14] Weiss, Andreas. "Volumetric Expander Versus Turbine – Which Is The Better Choice For Small Orc Plants?" *3 Rd International Seminar on ORC Power Systems* (2015).
- [15] Lemort, Vincent. "A Comparison Of Piston, Screw And Scroll Expanders For Small Scale Rankine Cycle Systems." *Thermodynamics Laboratory University of Leige* (2009).
- [16] Imran, Muhammad. "Volumetric Expanders for Low Grade Heat and Waste Heat Recovery Applications." *Renewable and Sustainable Energy Reviews* 57 (2016): 1090-1109.
- [17] Kolasiński, Piotr. "The Influence of the Heat Source Temperature on the Multivane Expander Output Power in an Organic Rankine Cycle (ORC) System." *Energies* 8 (2015): 3351-3369.

- [18] Papes, Iva. "Analysis of a Twin Screw Expander for ORC Systems Using Computational Fluid Dynamics with a Real Gas Model." International Compressor Engineering Conference (2014).
- [19] Stosic, Nikola. "Screw Expanders Increase Output and Decrease the Cost of Geothermal Binary Power Plant Systems." City University.
- [20] Kane, M. "Scroll Expander Organic Rankine Cycle (ORC) Efficiency Boost of Biogas Engines." Industrial Energy Systems Laboratory.
- [21] Cengel, Yunus, and Michael Boles. Thermodynamics: An Engineering Approach. 5th ed.
- [22] Hsu, Sung-Wei. "Experimental Investigation of the Performance of a Hermetic Screw-Expander Organic Rankine Cycle." Energies 7. 6172-6185.
- [23] Nils P. Halm. Mathematical modeling of scroll compressors. Master thesis of Herrick lab, School of Mechanical Engineering, Purdue University, 1997.
- [24] Chen, Y. "A Comprehensive Model of Scroll Compressors Part I: Compression Process Modeling." International Compressor Engineering Conference (2000).
- [25] Ziviani, David. "Comprehensive Model of a Single-screw Expander for ORC-Systems." International Compressor Engineering Conference (2014).
- [26] Glavatskaya, Yulia. "Reciprocating Expander for an Exhaust Heat Recovery Rankine Cycle for a Passenger Car Application." Energies 5 (2012).
- [27] Lopez, Eduardo. "Study On A Radial Turbine Stage With Inlet Guide Vanes For An Orc Process With An Electrical Output Of 3,5 KW." Master's Thesis (2013).
- [28] Cengel, Yunus, and Afshin Ghajar. Heat and Mass Transfer. 4th ed. New York: Mcgraw-Hill, 2007. Print.

- [29] Luhan, L. M. "Model Approximation to an Equation of State for the R245fa Fluid in an Expansion Process." *Applied Thermal Engineering* (2012).
- [30] Meng, Xianyang. "Compressed Liquid Viscosity of 1,1,1,3,3-Pentafluoropropane (R245fa) and 1,1,1,3,3,3-Hexafluoropropane (R236fa)." *Journal of Chemical and Engineering Data* 56 (2011): 4956-4964.
- [31] Zyhowski, G. J. "An Overview Of The Properties And Applications of HFC-245fa." *International Refrigeration and Air Conditioning Conference* (2002).
- [32] Disconzi, Fernanda P. "Development of an In-Cylinder Heat Transfer Correlation for Reciprocating Compressors." *International Compressor Engineering Conference* (2012).
- [33] Scott, T. C. *Derivation in Terms of Density and Pressure*. 1989. Print.
- [34] Gnutek, Z. and Kalinowski, E., "The Effect of Variations in the Amount of Working Medium Contained Within the Working Chamber on the Operation of a Rotary-Vane Vacuum Pump" (1998). *International Compressor Engineering Conference*. Paper 1240.
- [35] Brummer, Andreas. "Energy Efficiency – Waste Heat Utilization with Screw Expanders." *Pumps, Compressors and Process Components* (2012): 120-26.
- [36] Yang, Wong Young. *Applied Numerical Methods Using Matlab*. 2005. Print.
- [37] Wang XD, Zhao L, Wang JL, Zhang WZ, Zhao XZ, Wu W. Performance evaluation of a low-temperature solar Rankine cycle system utilizing R245fa. *Solar Energy* 2010;84:353–64.
- [38] Jiang Y, Ma Y, Fu L, Li M. Some design features of CO₂ two-rolling piston expander. *Energy* 2013;55:916–24.

- [39] Hua T, Yitai M, Minxia L, Haiqing G, Zhongyan L. Influence of a non- condensable gas on the performance of a piston expander for use in carbon dioxide trans-critical heat pumps. *Appl Therm Eng* 2011;31:1943–9.
- [40] Haiqing G, Yitai M, Minxia L. Some design features of CO₂ swing piston expander. *Appl Therm Eng* 2006;26:237–43.
- [41] Subiantoro A, Yap KS, Ooi KT. Experimental investigations of the revolving vane (RV-I) expander. *Appl Therm Eng* 2013;50:393–400.
- [42] M.b.Mohd. Tahir, N. Yamada and T.Hoshino. "Efficiency of a Compact Organic Rankine Cycle System with Rotary-Vane-Type Expander for Low-Temperature Waste Heat 183 Recovery," *International Journal of Civil Environmental Engineering*, vol. 2, no. 1, pp. 11- 16, 2010.
- [43] Zhang Y. Experimental study on the performance of single screw expander with 195 mm diameter screw. In: *Proceedings of the ASME ORC 2013 2nd International Seminar ORC Power System Rotterdam, Netherlands; 2013.*
- [44] Tatushi K, Naomichi H. Study of fundamental performance of helical screw expanders. *Japan Soc Mech Eng* 1985;28:1970–7.
- [45] Zhou N, Wang X, Chen Z, Wang Z. Experimental study on organic rankine cycle for waste heat recovery from low-temperature flue gas. *Energy* 2013;55:216–25.
- [46] Refrigerants, Honeywell. "Genetron® 245fa." Products. Web.
- [47] Lemort, V., S. Declaye and S. Quoilin. 2012. Experimental characterization of a hermetic scroll expander for use in a micro-scale Rankine cycle. *Proceedings of the Institution of Mechanical Engineers, Part A, Journal of Power and Energy*, Volume 226 Issue 1, February 2012.

- [48] Harada, Kevin. "Development of a Small Scale Scroll Expander." Master's Thesis (2011)
- [49] "Engineering ToolBox." Engineering ToolBox. N.p., n.d. Web. Sept. 2016.
- [50] Hsu, Sung-Wei, Hsiao-Wei Chiang, and Chih-Wei Yen. "Experimental Investigation of the Performance of a Hermetic Screw-Expander Organic Rankine Cycle." *Energies* 7.9 (2014): 6172-6185.
- [51] Stosic, N. "On Heat Transfer in Screw Compressors." *International Journal of Heat and Fluid Flow* 51 (2015): 285-297.
- [52] Stosic, Nikola, Ian K. Smith, and Ahmed Kovacevic. "Numerical and Experimental Research in Heat Transfer to Screw Compressor Rotors." *ASME/JSME 2011 8th Thermal Engineering Joint Conference* 2011.
- [53] Jang, Kitae, and Sangkwon Jeong. "Experimental Investigation on Convective Heat Transfer Mechanism in a Scroll Compressor." *International Journal of Refrigeration* 29.5 (2006): 744-753.
- [54] "Thermocouples." Omega. Omega Engineering, n.d. Web.
- [55] "UNIK 5000 Silicon Pressure Sensor." GE Measurement. General Electric, n.d. Web.
- [56] "Comparative Analysis of Thermal Time Constants in Iron-Core and Ironless-Armature DC Servo Motors ." Danaher Motion. N.p., 19 Nov. 2003. Web.

Vita Autoris

Name: Luka Celic

Place of Birth: Windsor, Ontario

Year of Birth: 1991

Education: M.A.Sc in Mechanical Engineering
University of Windsor, 2014-2016

Laurea Magistrale in Automotive Engineering
Politecnico di Torino, 2014-2016

B.A.Sc in Mechanical Engineering
University of Windsor, 2010-2014